Enhancing the Downlink Rate Fairness of Low-Resolution Active RIS-Aided Signaling by Closed-Form Expression-Based Iterative Optimization

Y. Chen[1], H. D. Tuan[2], Y. Fang[1], H. Yu[1], H. V. Poor[3], and L. Hanzo[4]

***Abstract*—This paper proposes a joint design strategy for enhancing individual user rates in a multi-user system by optimizing both the programmable reflecting elements (PREs) of an active reconfigurable intelligent surface (aRIS) and the transmit beamforming at a base station. Given that the aRIS's PREs are bound by discrete constraints due to low-resolution quantization, this design approach relies on large-scale mixed discrete-continuous problems, which are addressed through a new universal penalised optimization reformulations. Initially, we develop iterations based on convex quadratic solvers (CQ) to tackle the problem of maximizing the users' minimum rate (MR). Given that the computational complexity of these CQs is cubic, leading to high costs in large-scale computations, we introduce a pair of surrogate objectives. These objectives are designed in a way that their constrained optimization can be efficiently managed through iterations of closed-form expressions with scalable complexity, rendering them practical for large-scale computations. This pair of surrogate objectives comprises the maximization of the geometric mean of users' rates (GM-rate maximization) and the soft-maximization of users' MR (soft max-min rate optimization). Remarkably, they not only enhance MR but also contribute to the improvement of the sum-rate (SR). Building upon the GM-rate optimization, we further propose addressing the energy efficiency problem, which achieves a high ratio of SR to power consumption and MR to power dissipation through closed-form expressions. Comprehensive simulations are conducted to validate the efficacy of the proposed solutions.**

***Index Terms*—Active reconfigurable intelligent surface (aRIS), low-resolution quantization, transmit beamforming, active power control, max-min rate optimization, large-scale computation, mixed discrete continuous optimization.**

I. Introduction

Reconfigurable Intelligent Surfaces (RISs) have the potential to enhance the performance of next-generation wireless networks [1]–[3]. In contrast to traditional signal relaying methods, RISs utilize their programmable reflecting elements (PREs) to passively manipulate the incident waves, directing them towards the desired destinations [4]. However, without power amplification, the signals reaching the destination experience increased path-loss due to dual-hop propagation [5], causing a weakening compared to a single hop. Hence RIS-assisted twice-hop signaling, which involves optimizing both the RIS PREs and transmit beamformer weights, only proves advantageous in scenarios where no direct paths exist between the source and destination [6]–[8].

As a remedy, the concept of active RISs (aRISs), relying on power amplification at the RISs, has recently been proposed [9], [10]. Furthermore, aRIS-assisted signaling has also been explored extensively to improve the joint communication and sensing performance, as discussed in [10]–[17]. Unlike RISs, aRISs actively reflect signals with the aid of power amplification. By employing a modest amount of power for signal power amplification, they hold the promise of boosting the signals at the receiving end to mitigate the twin-hop path-loss. Research highlighted in [10] has shown that allocating merely 1% of the total transmit power to the aRIS PREs can significantly enhance the multi-user sum rate (MU SR).

Notably, aRIS-assisted signaling aiming for maximizing the MU SR has also been explored [14], [15], proposing an ad hoc approach to represent the SR function, akin to [10]. However, this ad hoc method can potentially exacerbate the nonlinearity of the objective function and necessitate an additional alternating optimization step. As a result, it is inadequate for addressing the individual user rate constraints. Moreover, the stand-alone MU SR maximization cannot guarantee MU rate-fairness and thus it is unsuitable for MU services, because it assigns a major portion of the optimized SR to users having favorable channel conditions, while serving other users with zero or near-zero rates. Notably, aRIS-assisted signaling optimization is remarkably simpler in comparison to its conventional (passive) RIS-assisted counterpart, when unquantized PREs are employed. This simplicity arises from the absence of computationally intricate unit modulus constraints (UMCs) applied to passive RIS's PREs. Consequently, the optimization problems for aRIS-assisted signaling closely

The work was supported in part by the Australian Research Council's Discovery Projects under Grant DP190102501, in part by the Shanghai Sailing Scholar under Grant 23YF1412700, in part by the Innovation Program of Shanghai Municipal Science Technology Commission under Grant 22511103202, in part by the U.S National Science Foundation under Grants CNS-2128448 and ECCS-2335876, in part by the Engineering and Physical Sciences Research Council projects EP/W016605/1, EP/X01228X/1 and EP/Y026721/1 as well as of the European Research Council's Advanced Fellow Grant QuantCom (Grant No. 789028)

[1]School of Communication and Information Engineering, Shanghai University Shanghai 200444, China (email: cyf119@shu.edu.cn, yfang@shu.edu.cn, hw_yu@shu.edu.cn); [2]School of Electrical and Data Engineering, University of Technology Sydney, Broadway, NSW 2007, Australia; [3]Department of Electrical and Computer Engineering, Princeton University, Princeton, NJ 08544, USA (email: poor@princeton.edu); [4]School of Electronics and Computer Science, University of Southampton, Southampton, SO17 1BJ, UK (email: lh@ecs.soton.ac.uk) (Corresponding Author: H. Yu)

resemble those of conventional multi-user relay-assisted signaling, which have been effectively tackled using convex-quadratic (CQ) solver-based path-following algorithms [18]–[23]. Applying CQ-based algorithms initially developed for passive RIS-assisted signaling [6] to solve problems related to aRIS-assisted signaling, including stand-alone SR maximization, SR maximization with MU rate-constraints, and max-min rate optimization, which were straightforward. In summary, the challenges associated with aRIS-assisted signaling using unquantized PREs are aligned with extensively studied categories in the existing literature. However, it is crucial to highlight that practical implementations predominantly employ PREs of low resolutions, operating within restricted discrete sets of configurations. Consequently, optimizing aRIS-assisted signaling poses significant computational challenges, involving large-scale mixed discrete-continuous problems that have not been thoroughly studied as yet.

Given the context outlined above, we will now delve into addressing the complex unresolved issue of achieving enhanced multi-user rate fairness through aRIS-assisted signaling, while utilizing low-resolution quantized PREs. Our contributions are three-fold.

- This is the first contribution solving the problem of maximizing the users' minimum rates (MR optimization), which constitutes a non-smooth mixed continuous discrete problem subject to discrete constraints arising from the low-resolution quantization of the PREs. Specifically, we develop a CQ-based algorithm for its solution;
- The second contribution pertains to the computational optimization challenges in aRIS-assisted signaling, primarily due to the substantial number of decision variables involved in optimizing both the MU beamformers and the PREs. Given the cubic increase in computational complexity for large-scale CQ problems, it is crucial to establish more flexible surrogate problems instead of direct MR optimization to achieve rate-fairness. This approach makes large-scale computations more manageable. Inspired by [7], the work [24] has demonstrated that the maximization of the geometric mean of the users' rates (GM-rate) leads to a Pareto-optimal solution, achieving both high SR and high MR. However, this GM-rate optimization remains computationally complex for aRIS-assisted systems. To address this, we capitalize on the smoothness of the GM-rate objective function and conceive iterative closed-form expressions of scalable complexity for its solution. We validate its Pareto optimality through simulations. Additionally, we devise a closed-form expression-based algorithm for optimizing the energy efficiency (EE) of the aRIS;
- We introduce an alternative surrogate optimization objective based on a soft and smooth approximation of the non-smooth MR function, which we also solve through iterative closed-form expressions of scalable complexity. Our simulations demonstrate that its solution achieves SR and MR outcomes similar to those obtained by directly maximizing the SR and MR, respectively.

We introduce Table I to clearly differentiate our contributions from related works. The last three rows highlight the distinctive aspects of our paper. A byproduct of this paper is a novel methodology which leads itself to addressing large-scale mixed discrete-continuous problems associated with MU rates.

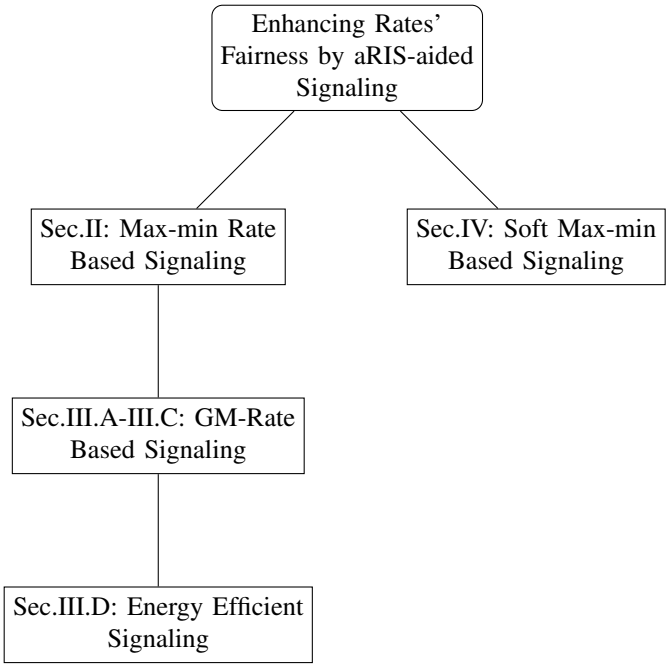

Fig. 1: The diagrammatic outline of the paper

The paper is organized as follows. Section II details the development of a CQ-based algorithm to solve the MR problem. In Section III, we introduce closed-form algorithms for the GM-rate and GM-rate-based EE problems. Additionally, we introduce and solve the soft max MR problem using a closed-form expression-based algorithm in Section IV. Section V presents our simulations and outlines our computational experiences. Lastly, Section VI concludes the paper. Appendix I reviews the relevant concepts of tight minorants and majorants [25], which play a pivotal role in the convergence of our optimization algorithms. Appendix II introduces an innovative bisection procedure of scalable complexity for solving multi-constrained quadratic programming. Fig. 1 offers a concise overview of the paper's main highlights at a glance.

Notation. Only variables stand out in boldface to emphasize to reveal useful structure for optimization. $\mathcal{C}(0, \sigma I)$ is the set of circular Gaussian random variables with zero means and variance σI. $\mathsf{diag}[z_m]_{m\in\mathcal{M}}$ for $\mathcal{M} \triangleq \{1, \ldots, M\}$ is the diagonal matrix with $z_1, \ldots, z_M$ on its diagonal.

II. Max-min rate optimization by convex-solver based computation

We consider the wireless network illustrated by Fig. 2, where an active RIS (aRIS) assists a base station (BS) having N elements to an antenna array with serve K single-antenna users, which are indexed by $k \in \mathcal{K} \triangleq \{1, \ldots, K\}$. The aRIS is equipped with M power-amplified programable reconfigurable

TABLE I: The paper's contributions.

Contents \ Literature	**This work**	[6]	[7]	[8]	[10]	[14]	[15]	[17]
Active RIS	√				√	√	√	√
Low-resolution PRE	√			√			√	
QoS	√	√	√	√		√	√	
Algorithm's convergence	√	√	√	√	√			
Multi-objective optimization	√							
QoS aware EE	√							
Tractable large scale computation	√							

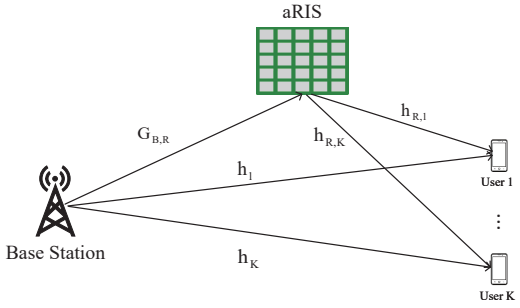

Fig. 2: aRIS-assisted signaling model

elements (APREs) $\mathbf{z}_m, m \in \mathcal{M} \triangleq \{1, \ldots, M\}$. We thus define the vector of APREs by

$$\mathbf{z} \triangleq \begin{bmatrix} \mathbf{z}_1 & \ldots & \mathbf{z}_M \end{bmatrix}^T \in \mathbb{C}^M. \quad (1)$$

Let us introduce

$$\mathbb{C}^{1\times M} \ni h_{R,k} \quad \& \quad G_{B,R} = \begin{bmatrix} G_{B,R,1} \\ \ldots \\ G_{B,R,M} \end{bmatrix} \in \mathbb{C}^{M\times N}, \quad G_{B,R,m} \in \mathbb{C}^{1\times N}, m \in \mathcal{M}, \quad (2)$$

to represent the channel spanning from the aRIS to user $k \in \mathcal{K}$, and that from the BS to aRIS. Furthermore, let $h_k \in \mathbb{C}^{1\times N}$ be the direct channel from the BS to user k. Then the two-path channel spanning from the BS to user k is given by

$$\tilde{h}_k(\mathbf{z}) \triangleq h_k + \hbar_k(\mathbf{z}), \quad (3)$$

where $\hbar_k(\mathbf{z})$ is the composite channel spanning from the BS to user k via the aRIS defined by

$$\mathbb{C}^{1\times M} \ni \hbar_k(\mathbf{z}) \triangleq h_{R,k} R_{R,k}^{1/2} \mathsf{diag}[\mathbf{z}_m]_{m\in\mathcal{M}} G_{B,R} \quad (4)$$

$$= \mathbf{z}^T \Delta_k, \quad (5)$$

where $R_{R,k}$ is the spatial correlation matrix of the RIS elements with respect to user k, while $\tilde{h}_{R,k} \triangleq h_{R,k} R_{R,k}^{1/2}$, and

$$\mathbb{C}^{M\times N} \ni \Delta_k \triangleq \mathsf{diag}[\tilde{h}_{BR,k}(m)]_{m\in\mathcal{M}} G_{B,R}, k \in \mathcal{K}. \quad (6)$$

To emphasize the performance enhancement of the proposed network, we assume perfect knowledge of the channel state information (CSI) through accurate channel estimation [26]–[28].

For supporting the practical implementation of an aRIS, we assume that the PREs are of low resolution, so the associated constraints are

$$\mathbf{z}_m = \boldsymbol{p}_m e^{\jmath \boldsymbol{\theta}_m}, m \in \mathcal{M}, \quad (7)$$

with $\boldsymbol{p}_m \in \mathbb{R}$ defining the power amplification coefficients, and

$$\boldsymbol{\theta}_m \in \mathcal{B} \triangleq \left\{ \beta \frac{2\pi}{2^b}, \beta = 0, 1, \ldots, 2^b - 1 \right\}, m \in \mathcal{M}, \quad (8)$$

defining the PREs of b-bit resolution.

Let $s_k \in \mathcal{C}(0,1)$ associated with $\mathbb{E}(|s_k|^2) = 1$ represent the information intended for user k, which is beamformed by the weight vector $\mathbf{w}_k \in \mathbb{C}^N$ before its downlink (DL) transmission from the BS. The signal received by user k can be written as

$$y_k = \tilde{\hbar}_k(\mathbf{z}) \sum_{k\in\mathcal{K}} \mathbf{w}_k s_k + \tilde{h}_{R,k} \mathsf{diag}[\mathbf{z}_m]_{m\in\mathcal{M}} \nu + n_k, \quad (9)$$

where $\nu \in \mathcal{C}(0, \sigma_\nu I)$ is the dynamic noise induced by aRIS, while $n_k \in \mathcal{C}(0, \sigma)$ is the additive white Gaussian noise (AWGN), which includes not only the background noise, but also the channel impairments due to having imperfect CSI knowledge [29].

The rate for user k is expressed as

$$r_k(\mathbf{w}, \mathbf{z}) = \ln\left(1 + \frac{|\tilde{\hbar}_k(\mathbf{z})\mathbf{w}_k|^2}{\varphi_k(\mathbf{w}, \mathbf{z})}\right), \quad (10)$$

with

$$\varphi_k(\mathbf{w},\mathbf{z}) \triangleq \sum_{j\in\mathcal{K}\setminus\{k\}} |\tilde{\hbar}_k(\mathbf{z})\mathbf{w}_j|^2 + \sigma_\nu \sum_{m\in\mathcal{M}} |\tilde{h}_{R,k}(m)|^2 |\mathbf{z}_m|^2 + \sigma = \sum_{j\in\mathcal{K}\setminus\{k\}} |\tilde{\hbar}_k(\mathbf{z})\mathbf{w}_j|^2 + \sigma_\nu \mathbf{z}^H \mathcal{D}_k \mathbf{z} + \sigma, \quad (11)$$

for

$$\mathcal{D}_k \triangleq \mathsf{diag}[|\tilde{h}_{R,k}(m)|^2]_{m\in\mathcal{M}}, k \in \mathcal{K}. \quad (12)$$

We also use (5) and (6) to represent

$$\tilde{\hbar}_k(\mathbf{z})\mathbf{w}_j = h_k \mathbf{w}_j + \mathbf{w}_j^T \Delta_k^T \mathbf{z}. \quad (13)$$

For $\mathbf{w} \triangleq \{\mathbf{w}_k, k \in \mathcal{K}\}$, the beamforming power constraint given the budget P is

$$\sum_{k\in\mathcal{K}} ||\mathbf{w}_k||^2 \leq P, \quad (14)$$

while the constraint of the reflected power at the aRISs is formulated as

$$\sum_{k\in\mathcal{K}} ||\mathsf{diag}[\mathbf{z}_m]_{m\in\mathcal{M}} G_{B,R} \mathbf{w}_k||^2 + \sigma_\nu ||\mathsf{diag}[\mathbf{z}_m]_{m\in\mathcal{M}}||^2 \leq P_A \quad (15)$$

$$\Leftrightarrow \quad \sum_{k\in\mathcal{K}} (\mathbf{w}_k)^H \mathcal{Q}_1(\mathbf{z}) \mathbf{w}_k \leq P_1(\mathbf{z}) \quad (16)$$

$$\Leftrightarrow \quad \mathbf{z}^H \mathcal{Q}_2(\mathbf{w}) \mathbf{z} \leq P_A, \quad (17)$$

where we have:

$$\begin{aligned} \mathcal{Q}_1(\mathbf{z}) &\triangleq (G_{B,R})^H \mathsf{diag}[|\mathbf{z}_m|^2]_{m\in\mathcal{M}} G_{B,R} \\ P_1(\mathbf{z}) &\triangleq P_A - \sigma_\nu ||\mathbf{z}||^2, \\ \mathcal{Q}_2(\mathbf{w}) &\triangleq \textstyle\sum_{k\in\mathcal{K}} \mathsf{diag}[|G_{B,R,m}\mathbf{w}_k|^2]_{m\in\mathcal{M}} + \sigma_\nu I_M. \end{aligned} \tag{18}$$

Note that Equation (16) expresses the reflected power constraint (15) as a convex quadratic constraint in $\mathbf{w}$ with $\mathbf{z}$ held fixed. Similarly, Equation (17) expresses the reflected power constraint (15) as a convex quadratic constraint in $\mathbf{z}$ with $\mathbf{w}$ held fixed.

To address the multi-user rate-fairness offered by aRIS-assisted communications, we consider the following max-min rate optimization problem:

$$\max_{\mathbf{w},\mathbf{z},\boldsymbol{\theta},\boldsymbol{p}} f(\mathbf{w},\mathbf{z}) \triangleq \min_{k\in\mathcal{K}} r_k(\mathbf{w},\mathbf{z}) \text{ s.t } (7),(8),(14),(15), \tag{19}$$

which is computationally challenging because its objective function is neither nonconcave nor nonconvex as well as non-smooth. Furthermore, (7) is a nonlinear equality constraint, while (8) is a difficult discrete constraint. We now follow [30] to address (19) via the following penalized optimization problem

$$\max_{\mathbf{w},\mathbf{z},\boldsymbol{\theta},\boldsymbol{p}} f_\rho(\mathbf{w},\mathbf{z},\boldsymbol{p},\boldsymbol{\theta}) \triangleq \left[f(\mathbf{w},\mathbf{z}) - \rho \sum_{m\in\mathcal{M}} |\mathbf{z}_m - \boldsymbol{p}_m e^{\jmath\boldsymbol{\theta}_m}|^2 \right] \quad \text{s.t} \quad (8),(14),(15), \tag{20}$$

where $\rho > 0$ is a penalty parameter introduced for incorporating the nonlinear equality constraint (7) into the optimization objective.

This section develops a convex solver based algorithm for the solution of the problem (20). Following initialization by a feasible point $(w^{(0)}, z^{(0)}, p^{(0)}, \theta^{(0)})$ for (20), let $(w^{(\kappa)}, z^{(\kappa)}, p^{(\kappa)}, \theta^{(\kappa)})$ be a feasible point for (20) that is found from the $(\kappa-1)$-st iteration. We now present alternating ascents in each of $\mathbf{w}$, $\mathbf{z}$, $\boldsymbol{p}$ and $\boldsymbol{\theta}$.

A. Beamforming ascent

To seek $w^{(\kappa+1)}$ so that

$$\begin{aligned} & f_\rho(w^{(\kappa+1)}, z^{(\kappa)}, p^{(\kappa)}, \theta^{(\kappa)}) > f_\rho(w^{(\kappa)}, z^{(\kappa)}, p^{(\kappa)}, \theta^{(\kappa)}) \\ \Leftrightarrow \quad & f(w^{(\kappa+1)}, z^{(\kappa)}) > f(w^{(\kappa)}, z^{(\kappa)}), \end{aligned} \tag{21}$$

we consider the following problem

$$\max_{\mathbf{w}} \; f_1^{(\kappa)}(\mathbf{w}) \triangleq \min_{k\in\mathcal{K}} r_{1,k}^{(\kappa)}(\mathbf{w}) \quad \text{s.t.} \quad (14), \tag{22a}$$

$$\sum_{k\in\mathcal{K}} (\mathbf{w}_k)^H \mathcal{Q}_1^{(\kappa)} \mathbf{w}_k \le P_1^{(\kappa)}, \tag{22b}$$

with $\mathcal{Q}_1^{(\kappa)} \triangleq \mathcal{Q}_1(z^{(\kappa)})$ and $P_1^{(\kappa)} \triangleq P_1(z^{(\kappa)})$ according to (16) and (18), while according to (10) and (11), we have:

$$r_{1,k}^{(\kappa)}(\mathbf{w}) \triangleq r_k(\mathbf{w}, z^{(\kappa)}) = \ln\left(1 + \frac{|h_{1,k}^{(\kappa)}\mathbf{w}_k|^2}{\varphi_{1,k}^{(\kappa)}(\mathbf{w})}\right), k \in \mathcal{K}. \tag{23}$$

for

$$\varphi_{1,k}^{(\kappa)}(\mathbf{w}) \triangleq \varphi_k(\mathbf{w}, z^{(\kappa)}) = \sum_{j\in\mathcal{K}\setminus\{k\}} |h_{1,k}^{(\kappa)}\mathbf{w}_j|^2 + \sigma_{1,k}^{(\kappa)},$$

and $h_{1,k}^{(\kappa)} \triangleq \tilde{h}_k(z^{(\kappa)})$, and

$$\sigma_{1,k}^{(\kappa)} \triangleq \sigma_\nu \sum_{m\in\mathcal{M}} |\tilde{h}_{R,k}(m)|^2 |z_m^{(\kappa)}|^2 + \sigma.$$

By applying the inequality (96) of Appendix I for $(\mathbf{v},\mathbf{y}) = [h_{1,k}^{(\kappa)}\mathbf{w}_k, \varphi_{1,k}^{(\kappa)}(\mathbf{w})]$ and $(\bar{v},\bar{y}) = [v_{1,k}^{(\kappa)}, y_{1,k}^{(\kappa)}] \triangleq (h_{1,k}^{(\kappa)} w_k^{(\kappa)}, \varphi_{1,k}^{(\kappa)}(w^{(\kappa)}))$, the following tight concave quadratic minorant of $r_{1,k}^{(\kappa)}(\mathbf{w})$ is obtained at $w^{(\kappa)}$:

$$\begin{aligned} \tilde{r}_{1,k}^{(\kappa)}(\mathbf{w}) \quad &\triangleq \\ a_{1,k}^{(\kappa)} + \frac{2}{y_{1,k}^{(\kappa)}} \Re\{(v_{1,k}^{(\kappa)})^* h_{1,k}^{(\kappa)} \mathbf{w}_k\rangle\} - \zeta_{1,k}^{(\kappa)} \sum_{j\in\mathcal{K}} |h_{1,k}^{(\kappa)}\mathbf{w}_j|^2 \quad &= (24) \\ a_{1,k}^{(\kappa)} + 2\Re\{\psi_{1,k}^{(\kappa)}\mathbf{w}_k\} - \zeta_{1,k}^{(\kappa)} \sum_{j\in\mathcal{K}} \mathbf{w}_j^H \Psi_{1,k}^{(\kappa)} \mathbf{w}_j, \quad &(25) \end{aligned}$$

with

$$a_{1,k}^{(\kappa)} \triangleq r_{1,k}^{(\kappa)}(w^{(\kappa)}) - \frac{|v_{1,k}^{(\kappa)}|^2}{y_{1,k}^{(\kappa)}} - \sigma_{1,k}^{(\kappa)}\zeta_{1,k}^{(\kappa)},$$

and

$$0 < \zeta_{1,k}^{(\kappa)} \triangleq \frac{|v_{1,k}^{(\kappa)}|^2}{y_{1,k}^{(\kappa)}\left(y_{1,k}^{(\kappa)} + |v_{1,k}^{(\kappa)}|^2\right)}$$

in (24), and $\psi_{1,k}^{(\kappa)} \triangleq (v_{1,k}^{(\kappa)})^* h_{1,k}^{(\kappa)} / y_{1,k}^{(\kappa)}$, and $\Psi_{1,k}^{(\kappa)} \triangleq (h_{1,k}^{(\kappa)})^H h_{1,k}^{(\kappa)}$, $k \in \mathcal{K}$ in (25).

We generate $w^{(\kappa+1)}$ by solving the following convex quadratic problem of tight minorant maximization:

$$\max_{\mathbf{w}} \min_{k\in\mathcal{K}} \tilde{r}_{1,k}^{(\kappa)}(\mathbf{w}) \quad \text{s.t.} \quad (14), (22b). \tag{26}$$

Since (26) involves KN decision variables and two quadratic constraints, its computational complexity of is on the order of $\mathcal{O}(K^3N^3)$.

Since $w^{(\kappa)}$ and $w^{(\kappa+1)}$ constitute a feasible point and the optimal solution for (26) respectively, we have:

$$\min_{k\in\mathcal{K}} \tilde{r}_{1,k}^{(\kappa)}(w^{(\kappa+1)}) > \min_{k\in\mathcal{K}} \tilde{r}_{1,k}^{(\kappa)}(w^{(\kappa)})$$

as far as $\min_{k\in\mathcal{K}} \tilde{r}_{1,k}^{(\kappa)}(w^{(\kappa)}) \neq \min_{k\in\mathcal{K}} \tilde{r}_{1,k}^{(\kappa)}(w^{(\kappa+1)})$. Therefore, we have:

$$\begin{aligned} f(w^{(\kappa+1)}, z^{(\kappa)}) &= \min_{k\in\mathcal{K}} r_{1,k}^{(\kappa)}(w^{(\kappa+1)}) \\ &\ge \min_{k\in\mathcal{K}} \tilde{r}_{1,k}^{(\kappa)}(w^{(\kappa+1)}) \quad (27) \\ &> \min_{k\in\mathcal{K}} \tilde{r}_{1,k}^{(\kappa)}(w^{(\kappa)}) \\ &= \min_{k\in\mathcal{K}} r_{1,k}^{(\kappa)}(w^{(\kappa)}) \quad (28) \\ &= f(w^{(\kappa)}, z^{(\kappa)}), \end{aligned}$$

verifying (21), where the inequality (27) and the equality (28) follow from the inequality $r_{1,k}^{(\kappa)}(w^{(\kappa+1)}) \ge \tilde{r}_{1,k}^{(\kappa)}(w^{(\kappa+1)})$ respectively and the equality $r_{1,k}^{(\kappa)}(w^{(\kappa)}) = \tilde{r}_{1,k}^{(\kappa)}(w^{(\kappa)})$, and the function $\tilde{r}_{1,k}^{(\kappa)}$ is a tight minorant of the function $r_{1,k}^{(\kappa)}$ at $w^{(\kappa)}$.

B. aRIS ascent

To seek $z^{(\kappa+1)}$ so that

$$f_\rho(w^{(\kappa+1)},z^{(\kappa+1)},p^{(\kappa)},\theta^{(\kappa)}) \;>\; f_\rho(w^{(\kappa+1)},z^{(\kappa)},p^{(\kappa)},\theta^{(\kappa)}), \tag{29}$$

we consider the following problem:

$$\max_{\mathbf{z}}\; f_{\rho,2}^{(\kappa)}(\mathbf{z}) \;\triangleq\; \left[\min_{k\in\mathcal{K}} r_{2,k}^{(\kappa)}(\mathbf{z}) -\rho\sum_{m\in\mathcal{M}}|\mathbf{z}_m - p_m^{(\kappa)}e^{\jmath\theta_m^{(\kappa)}}|^2\right] \tag{30a}$$

$$\text{s.t.}\quad \mathbf{z}^H\mathcal{Q}_2^{(\kappa)}\mathbf{z}\le P_A, \tag{30b}$$

with $\mathcal{Q}_2^{(\kappa)} \triangleq \mathcal{Q}_2(w^{(\kappa+1)})$ according to (17) and (18), while according to (6) and (13), we have:

$$r_{2,k}^{(\kappa)}(\mathbf{z}) \;\triangleq\; r_k(w^{(\kappa+1)},\mathbf{z}) \;=\; \ln\left(1+\frac{|\tau_{k,k}^{(\kappa)}+\Delta_{k,k}^{(\kappa)}\mathbf{z}|^2}{\varphi_{2,k}^{(\kappa)}(\mathbf{z})}\right), k\in\mathcal{K}, \tag{31}$$

with

$$\varphi_{2,k}^{(\kappa)}(\mathbf{z}) \;\triangleq\; \varphi_k(w^{(\kappa+1)},\mathbf{z}) \;=\; \textstyle\sum_{j\in\mathcal{K}\setminus\{k\}}|\tau_{k,j}^{(\kappa)}+\Delta_{k,j}^{(\kappa)}\mathbf{z}|^2+\sigma_\nu\mathbf{z}^H\mathcal{D}_k\mathbf{z}+\sigma,$$

and $\tau_{k,j}^{(\kappa)} \triangleq h_k w_j^{(\kappa+1)}$, $(k,j)\in\mathcal{K}\times\mathcal{K}$, and $\mathbb{C}^{1\times M}\ni\Delta_{k,j}^{(\kappa)}\triangleq (w_j^{(\kappa)})^T\Delta_k^T$, $(k,j)\in\mathcal{K}\times\mathcal{K}$, and $\mathcal{D}_k$ defined from (12).

Again, by applying the inequality (96) of Appendix I to $(\mathbf{v},\mathbf{y})\triangleq[\tau_{k,k}^{(\kappa)}+\Delta_{k,k}^{(\kappa)}\mathbf{z},\varphi_{2,k}^{(\kappa)}(\mathbf{z})]$ and $(\bar v,\bar y)=(v_{2,k}^{(\kappa)},y_{2,k}^{(\kappa)})\triangleq[\tau_{k,k}^{(\kappa)}+\Delta_{k,k}^{(\kappa)}z^{(\kappa)},\varphi_{2,k}^{(\kappa)}(z^{(\kappa)})]$, the following tight concave quadratic minorant of $r_{2,k}^{(\kappa)}(\mathbf{z})$ is obtained at $z^{(\kappa)}$:

$$\tilde r_{2,k}^{(\kappa)}(\mathbf{z}) \;\triangleq\; \tilde a_{2,k}^{(\kappa)}+\frac{2\Re\{(v_{2,k}^{(\kappa)})^*\left(\tau_{k,k}^{(\kappa)}+\Delta_{k,k}^{(\kappa)}\mathbf{z}\right)\}}{y_{2,k}^{(\kappa)}} -\zeta_{2,k}^{(\kappa)}\left(\sum_{j\in\mathcal{K}}|\tau_{k,j}^{(\kappa)}+\Delta_{k,j}^{(\kappa)}\mathbf{z}|^2+\sigma_\nu\mathbf{z}^H\mathcal{D}_k\mathbf{z}\right) \tag{32}$$

with

$$\tilde a_{2,k}^{(\kappa)} \triangleq r_{2,k}^{(\kappa)}(z^{(\kappa)})-\frac{|v_{2,k}^{(\kappa)}|^2}{y_{2,k}^{(\kappa)}}-\sigma\zeta_{2,k}^{(\kappa)},$$

and

$$0<\zeta_{2,k}^{(\kappa)}\triangleq\frac{|v_{2,k}^{(\kappa)}|^2}{y_{2,k}^{(\kappa)}\left(|v_{2,k}^{(\kappa)}|^2+y_2^{(\kappa)}\right)}.$$

By using the identity

$$|\tau_{k,j}^{(\kappa)}+\Delta_{k,j}^{(\kappa)}\mathbf{z}|^2=|\tau_{k,j}^{(\kappa)}|^2+2\Re\{(\tau_{k,j}^{(\kappa)})^*\Delta_{k,j}^{(\kappa)}\mathbf{z}\}+\mathbf{z}^H\tilde\Delta_{k,j}^{(\kappa)}\mathbf{z}$$

with

$$0\preceq\tilde\Delta_{k,j}^{(\kappa)}\triangleq(\Delta_{k,j}^{(\kappa)})^H\Delta_{k,j}^{(\kappa)},(k,j)\in\mathcal{K}\times\mathcal{K},$$

we represent (32) by

$$\tilde r_{2,k}^{(\kappa)}(\mathbf{z}) \;=\; \tilde a_{2,k}^{(\kappa)}+\frac{2\Re\{(v_{2,k}^{(\kappa)})^*\tau_{k,k}^{(\kappa)}\}}{y_{2,k}^{(\kappa)}}+\frac{2\Re\{(v_{2,k}^{(\kappa)})^*\Delta_{k,k}^{(\kappa)}\mathbf{z}\}}{y_{2,k}^{(\kappa)}} -\zeta_{2,k}^{(\kappa)}(\sum_{j\in\mathcal{K}}(|\tau_{k,j}^{(\kappa)}|^2+2\Re\{(\tau_{k,j}^{(\kappa)})^*\Delta_{k,j}^{(\kappa)}\mathbf{z}\}+\mathbf{z}^H\tilde\Delta_{k,j}^{(\kappa)}\mathbf{z}) +\sigma_\nu\mathbf{z}^H\mathcal{D}_k\mathbf{z}) \;=\; a_{2,k}^{(\kappa)}+2\Re\{\psi_{2,k}^{(\kappa)}\mathbf{z}\}+\mathbf{z}^H\Psi_{2,k}^{(\kappa)}\mathbf{z}, \tag{33}$$

for

$$a_{2,k}^{(\kappa)}\triangleq\tilde a_{2,k}^{(\kappa)}+\frac{2}{y_{2,k}^{(\kappa)}}\Re\{(v_{2,k}^{(\kappa)})^*\tau_{k,k}^{(\kappa)}\}-\zeta_{2,k}^{(\kappa)}\sum_{j\in\mathcal{K}}|\tau_{k,j}^{(\kappa)}|^2,$$

and

$$\psi_{2,k}^{(\kappa)}\triangleq\frac{(v_{2,k}^{(\kappa)})^*\Delta_{k,k}^{(\kappa)}}{y_{2,k}^{(\kappa)}}-\zeta_{2,k}^{(\kappa)}\sum_{j\in\mathcal{K}}(\tau_{k,j}^{(\kappa)})^*\Delta_{k,j}^{(\kappa)},$$

and

$$\Psi_{2,k}^{(\kappa)}\triangleq\zeta_{2,k}^{(\kappa)}\left(\sum_{j\in\mathcal{K}}\tilde\Delta_{k,j}^{(\kappa)}+\sigma_\nu\mathcal{D}_k\right).$$

We generate $z^{(\kappa+1)}$ by solving the following convex quadratic problem of tight minorant maximization at $z^{(\kappa)}$:

$$\max_{\mathbf{z}}\; \tilde f_{\rho,2}^{(\kappa)}(\mathbf{z})\triangleq\left[\min_{k\in\mathcal{K}}\tilde r_{2,k}^{(\kappa)}(\mathbf{z}) -\rho\sum_{m\in\mathcal{M}}|\mathbf{z}_m-p_m^{(\kappa)}e^{\jmath\theta_m^{(\kappa)}}|^2\right] \quad\text{s.t.}\quad (30b). \tag{34}$$

As (34) involves M decision variables, its computational complexity is on the order of $\mathcal{O}(M^3)$.

It follows that

$$\tilde f_{\rho,2}^{(\kappa)}(z^{(\kappa+1)})>\tilde f_{\rho,2}^{(\kappa)}(z^{(\kappa)})$$

as long as we have $\tilde f_{\rho,2}^{(\kappa)}(z^{(\kappa+1)})\neq\tilde f_{\rho,2}^{(\kappa)}(z^{(\kappa)})$, because $z^{(\kappa)}$ and $z^{(\kappa+1)}$ constitute a feasible point and the optimal solution for (34) respectively. Therefore, we have:

$$\begin{aligned} f_\rho(w^{(\kappa+1)},z^{(\kappa+1)},p^{(\kappa)},\theta^{(\kappa)}) &= f_{\rho,2}^{(\kappa)}(z^{(\kappa+1)}) \\ &\ge f_{\rho,2}^{(\kappa)}(z^{(\kappa+1)}) \qquad (35)\\ &> \tilde f_{\rho,2}^{(\kappa)}(z^{(\kappa)}) \\ &= f_{\rho,2}^{(\kappa)}(z^{(\kappa)}) \qquad (36)\\ &= f_\rho(w^{(\kappa+1)},z^{(\kappa)},p^{(\kappa)},\theta^{(\kappa)}), \end{aligned}$$

verifying (29), where the inequality (35) and the equality (36) follow from the inequality $r_{2,k}^{(\kappa)}(z^{(\kappa+1)})\ge r_{2,k}^{(\kappa)}(z^{(\kappa+1)})$ respectively and the equality $r_{2,k}^{(\kappa)}(z^{(\kappa)})=\tilde r_{2,k}^{(\kappa)}(z^{(\kappa)})$ as the function $\tilde r_{2,k}^{(\kappa)}$ is a tight minorant of the function $r_{2,k}^{(\kappa)}$ at $z^{(\kappa)}$.

C. Amplifier and PRE ascent

We generate $p^{(\kappa+1)}$ and $\theta^{(\kappa+1)}$ by

$$\begin{aligned} p_m^{(\kappa+1)} &= \arg\min_{\boldsymbol{p}_m}|z_m^{(\kappa+1)}-\boldsymbol{p}_m e^{\jmath\theta_m^{(\kappa)}}|^2 \\ &= |z_m^{(\kappa+1)}|\cos(\angle z^{(\kappa+1)}-\theta_m^{(\kappa)}), m\in\mathcal{M}, \end{aligned} \tag{37}$$

and[1]

$$\theta_m^{(\kappa+1)}=\arg\min_{\boldsymbol{\theta}_m\in\mathcal{B}}|z_m^{(\kappa+1)}-p_m^{(\kappa+1)}e^{\jmath\boldsymbol{\theta}_m}|^2=\lfloor\angle z_m^{(\kappa+1)}\rceil_b, \tag{38}$$

[1] $\lfloor\angle z_m^{(\kappa+1)}\rceil_b=\nu_b\frac{2\pi}{2^b}$ with $\nu_b\triangleq\arg\min_{\{\nu,\nu+1\}}\left|\nu\frac{2\pi}{2^b}-\angle z_m^{(\kappa+1)}\right|$ for $\angle z_m^{(\kappa+1)}\in[\nu\frac{2\pi}{2^b},(\nu+1)\frac{2\pi}{2^b}]$.

which yield

$$\begin{aligned} & f_\rho(w^{(\kappa+1)},z^{(\kappa+1)},p^{(\kappa+1)},\theta^{(\kappa+1)}) \\ > \; & f_\rho(w^{(\kappa+1)},z^{(\kappa+1)},p^{(\kappa+1)},\theta^{(\kappa)}) \\ > \; & f_\rho(w^{(\kappa+1)},z^{(\kappa+1)},p^{(\kappa)},\theta^{(\kappa)}). \end{aligned} \tag{39}$$

D. Algorithm and convergence

Algorithm 1 provides the pseudo code of solving problem (20). It follows from (21), (29) and (39) that

$$f_\rho(w^{(\kappa+1)},z^{(\kappa+1)},p^{(\kappa+1)},\theta^{(\kappa+1)}) > f_\rho(w^{(\kappa)},z^{(\kappa)},p^{(\kappa)},\theta^{(\kappa)}), \tag{40}$$

so the sequence $\{(w^{(\kappa)},z^{(\kappa)},p^{(\kappa)},\theta^{(\kappa)})\}$ of improved feasible points for (20) converges to $(\bar{w},\bar{z},\bar{p},\bar{\theta})$ by the Cauchy theorem. Furthermore, a sufficiently large $\rho>0$ guarantees that

$$\max_{m\in\mathcal{M}} |z_m^{(\kappa)} - p_m^{(\kappa)} e^{\jmath\theta_m^{(\kappa)}}|^2 \to 0 \quad \text{as} \quad \kappa\to\infty,$$

i.e. $\bar{z}_m = \bar{p}_m e^{\jmath\bar{\theta}_m}$, $m\in\mathcal{M}$, implying that $(\bar{z},\bar{p},\bar{\theta})$ satisfies the nonlinear constraint (7). Therefore, $(\bar{w},\bar{z},\bar{p},\bar{\theta})$ is feasible for (19). Actually, we can state that the four-tuple $(\bar{w},\bar{z},\bar{p},\bar{\theta})$ is at least its locally optimal solution [6].

Algorithm 1 CQ-based algorithm of cubic complexity for computing the MR problem (20)

1: **Initialization:** Randomly generate the four-tuple $(w^{(0)},z^{(0)},p^{(0)},\theta^{(0)})$ feasible for (20). Set $\kappa=0$.
2: **Repeat until convergence:** Generate $w^{(\kappa+1)}$ by solving the convex problem (26) of the complexity order $\mathcal{O}(K^3N^3)$, and $z^{(\kappa+1)}$ by solving the convex problem (34) of the complexity order $\mathcal{O}(M^3)$. Generate $(p^{(\kappa+1)},\theta^{(\kappa+1)})$ by (37)-(38). Reset $\kappa\leftarrow\kappa+1$.
3: **Output** $(w^{(\kappa)},z^{(\kappa)},p^{(\kappa)},\theta^{(\kappa)})$ and $r_k(w^{(\kappa)},)$, $k\in\mathcal{K}$.

III. GM-RATE MAXIMIZATION BY SCALABLE-COMPLEX CLOSED-FORMS AND APPLICATION TO TRACTABLE RATE-FAIRNESS AWARE ENERGY EFFICIENCY

The cubic computational complexity of each iteration of the CQ-based Algorithm 1 is $\mathcal{O}(K^3N^3)+\mathcal{O}(M^3)$, which is high because both KN and M are typically larger than 100. This section is the first step to resolve this computational issue in achieving the uniform MU rate-fairness by considering the following problem

$$\max_{\mathbf{w},\mathbf{z},\boldsymbol{p},\boldsymbol{\theta}} f_{GM}(\mathbf{w},\mathbf{z}) \triangleq \left(\prod_{k\in\mathcal{K}} r_k(\mathbf{w},\mathbf{z})\right)^{1/K} \quad \text{s.t.} \quad (7),(8),(14),(15), \tag{41}$$

which is termed as the GM-rate problem. Our previous treatises [7], [8], [24] have shown that GM-rate maximization provides a unique approach capable of achieving rate-fairness similar to that achieved by direct MR optimization as well as a competitive SR compared to that achieved by direct SR maximization.

Similarly to (19), we address (41) via the following penalized optimization problem:

$$\max_{\mathbf{w},\mathbf{z},\boldsymbol{p},\boldsymbol{\theta}} f_{\rho,GM}(\mathbf{w},\mathbf{z}) \quad \text{s.t.} \quad (8),(14),(15), \tag{42}$$

for $f_{\rho,GM}(\mathbf{w},\mathbf{z}) \triangleq \left[f_{GM}(\mathbf{w},\mathbf{z}) - \rho\sum_{m\in\mathcal{M}} |\mathbf{z}_m - \boldsymbol{p}_m e^{\jmath\boldsymbol{\theta}_m}|^2\right]$, which is still solved by Algorithm 1, while relying on the min objectives $\min_{k\in\mathcal{K}} \tilde{r}_{1,k}^{(\kappa)}(\mathbf{w})$ and $\min_{k\in\mathcal{K}} \tilde{r}_{2,k}^{(\kappa)}(\mathbf{z})$ in (26) and (34) are replaced by the GM-objectives $\left(\prod_{k\in\mathcal{K}} \tilde{r}_{1,k}^{(\kappa)}(\mathbf{w})\right)^{1/K}$ and $\left(\prod_{k\in\mathcal{K}} \tilde{r}_{2,k}^{(\kappa)}(\mathbf{z})\right)^{1/K}$, which are still concave, since they represent the GM of concave functions [25].

We now follow our previously developed procedures in [7], [8], [24] to conceive an algorithm of scalable complexity for its solution.

Initialized by a feasible point $(w^{(0)},z^{(0)},p^{(0)},\theta^{(0)})$ for (20), let $(w^{(\kappa)},z^{(\kappa)},p^{(\kappa)},\theta^{(\kappa)})$ be a feasible point for (42) that is found from the $(\kappa-1)$-st iteration. The corresponding ascent optimization is based on the problem:

$$\max_{\mathbf{w},\mathbf{z}} f_{\rho,GM}^{(\kappa)}(\mathbf{w},\mathbf{z}) \triangleq \Big[f_{GM}^{(\kappa)}(\mathbf{w},\mathbf{z}) - \rho\sum_{m\in\mathcal{M}} |\mathbf{z}_m - p_m^{(\kappa)} e^{\jmath\theta_m^{(\kappa)}}|^2\Big] \quad \text{s.t.} \quad (8),(14),(15), \tag{43}$$

where $f_{GM}^{(\kappa)}(\mathbf{w},\mathbf{z}) \triangleq \sum_{k\in\mathcal{K}} \lambda_k^{(\kappa)} r_k(\mathbf{w},\mathbf{z})$, for

$$\lambda_k^{(\kappa)} = \frac{\max_{k'\in\mathcal{K}} r_{k'}(w^{(\kappa)},z^{(\kappa)})}{r_k(w^{(\kappa)},z^{(\kappa)})}, k\in\mathcal{K}. \tag{44}$$

A. Beamforming ascent

To seek $w^{(\kappa+1)}$ so that

$$\begin{aligned} & f_{\rho,GM}^{(\kappa)}(w^{(\kappa+1)},z^{(\kappa)}) > f_{\rho,GM}^{(\kappa)}(w^{(\kappa)},z^{(\kappa)}) \\ \Leftrightarrow \quad & f_{GM}^{(\kappa)}(w^{(\kappa+1)},z^{(\kappa)}) > f_{GM}^{(\kappa)}(w^{(\kappa)},z^{(\kappa)}), \end{aligned} \tag{45}$$

we consider the following problem

$$\max_{\mathbf{w}} \; f_{GM,1}^{(\kappa)}(\mathbf{w}) \triangleq \sum_{k\in\mathcal{K}} \lambda^{(\kappa)} r_{1,k}^{(\kappa)}(\mathbf{w}) \quad \text{s.t.} \quad (14),(22b), \tag{46}$$

with $r_{1,k}^{(\kappa)}(\mathbf{w})$ defined from (23). Using (25), we obtain the following tight concave quadratic minorant of the objective function $f_{GM,1}^{(\kappa)}(\mathbf{w})$ in (46) at $w^{(\kappa)}$:

$$\begin{aligned} \tilde{f}_{GM,1}^{(\kappa)}(\mathbf{w}) \; & \triangleq \; \sum_{k\in\mathcal{K}} \lambda_k^{(\kappa)} \tilde{r}_{1,k}^{(\kappa)}(\mathbf{w}) \\ & = \; \sum_{k\in\mathcal{K}} \lambda_k^{(\kappa)} a_{1,k}^{(\kappa)} + 2\sum_{k\in\mathcal{K}} \Re\{\lambda_{1,k}^{(\kappa)} \psi_{1,k}^{(\kappa)} \mathbf{w}_k\} \\ & \quad - \sum_{k\in\mathcal{K}} (\mathbf{w}_k)^H \Psi_1^{(\kappa)} \mathbf{w}_k, \end{aligned} \tag{47}$$

with $0 \preceq \Psi_1^{(\kappa)} \triangleq \sum_{k\in\mathcal{K}} \lambda_k^{(\kappa)} \zeta_{1,k}^{(\kappa)} \Psi_{1,k}^{(\kappa)}$. We thus generate $w^{(\kappa+1)}$ verifying (45) by solving the following convex quadratic problem of tight minorant maximization at $w^{(\kappa)}$:

$$\max_{\mathbf{w}} \; \tilde{f}_{GM,1}^{(\kappa)}(\mathbf{w}) \quad \text{s.t.} \quad (14),(22b). \tag{48}$$

Utilizing a traditional convex solver results in a computational complexity of $\mathcal{O}(K^3N^3)$. Nevertheless, this problem falls within the problem class defined by (98) and can be solved using the innovative bisection approach with scalable complexity outlined in Appendix II.

B. aRIS ascent

To seek $z^{(\kappa+1)}$ so that

$$f^{(\kappa)}_{\rho,GM}(w^{(\kappa+1)},z^{(\kappa+1)}) > f^{(\kappa)}_{\rho,GM}(w^{(\kappa+1)},z^{(\kappa)}), \tag{49}$$

we consider the following problem

$$\max_{\mathbf{z}} f^{(\kappa)}_{\rho,GM2}(\mathbf{z}) \triangleq \left[f^{(\kappa)}_{GM2}(\mathbf{z}) - \rho \sum_{m\in\mathcal{M}} |\mathbf{z}_m - p^{(\kappa)}_m e^{\jmath\theta^{(\kappa)}_m}|^2 \right] \quad \text{s.t.} \quad (30b), \tag{50}$$

where $f^{(\kappa)}_{GM,2}(\mathbf{z}) \triangleq \sum_{k\in\mathcal{K}} \lambda^{(\kappa)} r^{(\kappa)}_{2,k}(\mathbf{z})$ with $r^{(\kappa)}_{2,k}(\mathbf{z})$ defined from (31).

Using (31), we obtain the following tight concave quadratic minorant of $f^{(\kappa)}_{GM,2}(\mathbf{z})$ in (50) at $z^{(\kappa)}$:

$$\begin{aligned} \tilde{f}^{(\kappa)}_{GM,2}(\mathbf{z}) &\triangleq \sum_{k\in\mathcal{K}} \lambda^{(\kappa)}_k \tilde{r}^{(\kappa)}_{2,k}(\mathbf{z}) \\ &= a^{(\kappa)}_2 + 2\Re\{\psi^{(\kappa)}_2 \mathbf{z}\} + \mathbf{z}^H \Psi^{(\kappa)}_2 \mathbf{z}, \end{aligned} \tag{51}$$

for $a^{(\kappa)}_2 \triangleq \sum_{k\in\mathcal{K}} \lambda^{(\kappa)}_k a^{(\kappa)}_{2,k}$, $\psi^{(\kappa)}_2 \triangleq \sum_{k\in\mathcal{K}} \lambda^{(\kappa)}_k \psi^{(\kappa)}_{2,k}$, and $\Psi^{(\kappa)}_2 \triangleq \sum_{k\in\mathcal{K}} \lambda^{(\kappa)}_k \Psi^{(\kappa)}_{2,k}$. We thus generate $z^{(\kappa+1)}$ verifying (49) by solving the following convex problem of tight minorant maximization:

$$\max_{\mathbf{z}} \left[\tilde{f}^{(\kappa)}_{GM,2}(\mathbf{z}) - \rho \sum_{m\in\mathcal{M}} |\mathbf{z}_m - p^{(\kappa)}_m e^{\jmath\theta^{(\kappa)}_m}|^2 \right] \quad \text{s.t.} \quad (30b). \tag{52}$$

Applying the Lagrangian multiplier method to solve our convex quadratic programming problem subject to a single quadratic constraint, we derive the following closed-form solution for (52):

$$z^{(\kappa+1)} = \begin{cases} (\Psi^{(\kappa)}_2 + \rho I_M)^{-1} \xi^{(\kappa)} \\ \text{if} \quad ||\sqrt{\mathcal{Q}^{(\kappa)}_2}(\Psi^{(\kappa)}_2 + \rho I_M)^{-1}\xi^{(\kappa)}||^2 \le P_A \\ (\Psi^{(\kappa)}_2 + \rho I_M + \alpha \mathcal{Q}^{(\kappa)}_2)^{-1}\xi^{(\kappa)} \quad \text{otherwise}, \end{cases}$$

where $\xi^{(\kappa)} \triangleq (\psi^{(\kappa)}_2)^H + \rho(p^{(\kappa)}_1 e^{\jmath\theta^{(\kappa)}_1}, \ldots, p^{(\kappa)}_M e^{\jmath\theta^{(\kappa)}_M})^T$ and $\alpha > 0$ is found by bisection, so that $||\sqrt{\mathcal{Q}^{(\kappa)}_2}(\Psi^{(\kappa)}_2 + \rho I_M + \alpha\mathcal{Q}^{(\kappa)}_2)^{-1}\xi^{(\kappa)}||^2 = P_A$.

C. Algorithm and its convergence

Algorithm 2 provides the pseudo code for solving the problem (42) based on iterating the closed forms (48), (53), (37), and (38). The reader is referred to [7], [8], [24] for a proof of its convergence.

Algorithm 2 GM algorithm of scalable complexity for computing the GM-rate problem (42)

1: **Initialization:** Randomly generate a feasible four-tuple $(w^{(0)}, z^{(0)}, p^{(0)}, \theta^{(0)})$ for (42). Set $\kappa = 0$.
2: **Repeat until convergence of the objective function in** (42)**:** Define $\lambda^{(\kappa)}_k$ by (44). Generate $w^{(\kappa+1)}$ by solving (48), $z^{(\kappa+1)}$ by (53). Generate $(p^{(\kappa+1)}, \theta^{(\kappa+1)})$ by (37)-(38). Reset $\kappa \leftarrow \kappa + 1$.
3: **Output** $(w^{(\kappa)}, z^{(\kappa)}, p^{(\kappa)}, \theta^{(\kappa)})$ and $r_k(w^{(\kappa)}, z^{(\kappa)})$, $k \in \mathcal{K}$.

D. Application to rate-fairness aware energy-efficiency

It is plausible that the κ-th iteration of solving the SR problem of

$$\max_{\mathbf{w},\mathbf{z},\boldsymbol{p},\boldsymbol{\theta}} f_{SR}(\mathbf{w},\mathbf{z}) \triangleq \sum_{k\in\mathcal{K}} r_k(\mathbf{w},\mathbf{z}) \quad \text{s.t.} \quad (7),(8),(14),(15), \tag{53}$$

is based on solving the problem (43) for $\lambda^{(\kappa)}_k \equiv 1$. Hence the SR problem (53) can be solved by Algorithm 2 upon setting $\lambda^{(\kappa)}_k \equiv 1$. The iterations based on (48) and (53), disregarding the constraints (7), (8) of low resolutions, have been precisely derived in [6], [31] and the novelty here lies in demonstrating that the problem (48) subject to a pair of convex quadratic constraints admits a closed-form expression based solution. Meanwhile, the SR problem (53) excluding (48) and (53) was tackled in [10], [14] using an ad hoc representation of the sum rate function $f_{SR}(\mathbf{w},\mathbf{z})$ by $\max_{\mathbf{y}\in\mathbb{R}^{2K}_+} F_{SR}(\mathbf{y},\mathbf{w},\mathbf{z})$. From a computational perspective, optimization of this function $F_{SR}(\mathbf{y},\mathbf{w},\mathbf{z})$ is no more computational tractable than $f_{SR}(\mathbf{w},\mathbf{z})$. Moreover, the former involves multiple superfluous variables $\mathbf{y}$, which contribute to the increased nonlinearity. The optimization in $(\mathbf{w},\mathbf{z})$ with $\mathbf{y}$ held fixed remains computationally intractable, necessitating an alternating optimization in $\mathbf{w}$ and in $\mathbf{z}$. Consequently, three alternating steps are employed. Although the SR problem (53) can be efficiently solved, it is deficient in MU communication, because it assigns a major portion of the optimal SR to a few users having favorable channel conditions, while leaving zero or almost zero rates for the other users. In other words, SR optimization without QoS constraints lacks meaningful implications.

In considering the following rate-fairness constrained energy efficiency (EE) problem

$$\max_{\mathbf{w},\mathbf{z}} \frac{f_{SR}(\mathbf{w},\mathbf{z})}{\pi(\mathbf{w},\mathbf{z})} \quad \text{s.t.} \quad (14),(15), \tag{54a}$$

$$r_k(\mathbf{w},\mathbf{z}) \ge \bar{\gamma}, k \in \mathcal{K}, \tag{54b}$$

where $\pi(\mathbf{w},\mathbf{z})$ is the total power consumption defined by

$$\begin{aligned} \pi(\mathbf{w},\mathbf{z}) = \tau_{BS} \sum_{k\in\mathcal{K}} ||\mathbf{w}_k||^2 + \tau_{RIS}[\sum_{k\in\mathcal{K}} ||\mathsf{diag}[\mathbf{z}_m]_{m\in\mathcal{M}} \\ \times G_{B,R}\mathbf{w}_k||^2 + \sigma_\nu ||\mathsf{diag}[\mathbf{z}_m]_{m\in\mathcal{M}}||^2] + P_{non}, \end{aligned} \tag{55}$$

the variable τ_{BS} (τ_{RIS}, resp.) represent to the reciprocal of the drain efficiency of the amplifier at the BS (RIS, resp.), and P_{non} is the total circuit power consumed at the BS and the RIS, the authors of [14] deprive the QoS constraint (54b) by

$$|\tilde{h}_k(\mathbf{z})\mathbf{w}_k|^2 / \varphi_k(\mathbf{w},\mathbf{z}) \ge (e^{\bar{\gamma}} - 1), k \in \mathcal{K}, \tag{56}$$

which are treated as convex quadratic constraints in $\mathbf{w}$ and $\mathbf{z}$ (see [14, (19b) and (20b)]). In fact, (56) represents the d.c. (difference of two convex functions) constraints in $\mathbf{w}$ or $\mathbf{z}$ that are not convex [25] but by [32], [33] it is equivalent to $\Re\{\tilde{h}_k(\mathbf{z})\mathbf{w}_k\} \ge \sqrt{e^{\bar{\gamma}} - 1}\sqrt{\varphi_k(\mathbf{w},\mathbf{z})}$ which is a second-order cone (SOC) in $\mathbf{w}$ and $\mathbf{z}$. Then, one can follow [22, Ineq. (A1)] or [34, Ineq. (68)] to obtain a tight minorant of the objective function in (54), which is concave quadratic in $\mathbf{w}$ and $\mathbf{z}$, for alternating descent iterations.

The authors of [15] considered the following RIS resolution and QoS constrained EE problem

$$\max_{\mathbf{w},\mathbf{z},\boldsymbol{p},\boldsymbol{\theta}} \frac{f_{SR}(\mathbf{w},\mathbf{z})}{\pi(\mathbf{w},\mathbf{z})} \quad \text{s.t.} \quad (7),(8),(14),(15),(54b), \tag{57}$$

which follows [6] to use the minorant $\tilde{r}_{1,k}^{(\kappa)}(\mathbf{w})$ and $\tilde{r}_{2,k}^{(\kappa)}(\mathbf{z})$ of $r_k(\mathbf{w},z^{(\kappa)})$ and $r_k(w^{(\kappa+1)},\mathbf{z})$ to handle the QoS constraint (54b) by its inner approximations $\tilde{r}_{1,k}^{(\kappa)}(\mathbf{w}) \geq \bar{\gamma}$ and

$$\tilde{r}_{2,k}^{(\kappa)}(\mathbf{z}) \geq \bar{\gamma}. \tag{58}$$

However, while its proposed alternating optimization in $\mathbf{w}$ looks correct, its alternating optimization in $\mathbf{z}$ [15, Alg. 1], which iterates by solving many convex problems in $\mathbf{z}$, does not result in a $z^{(\kappa+1)}$, which is feasible for (7), (8), and (58) due to the rate-fairness constraint (58). More explicitly, due to the QoS constraint (58), it may stop at $(z^{(\kappa+1)},p^{(\kappa+1)},\theta^{(\kappa+1)})$ with $|z_m^{(\kappa+1)}-p_m^{(\kappa+1)}e^{\jmath\theta_m^{(\kappa+1)}}|>0$ and thus it is infeasible for (7), (8), and (58).

To eliminating the rate-fairness constraint (54b) that causes intractable computation, as suggested in [35], the following problem is more appropriate

$$\max_{\mathbf{w},\mathbf{z}} \frac{\left(\prod_{k\in\mathcal{K}} r_k(\mathbf{w},\mathbf{z})\right)^{1/K}}{\pi(\mathbf{w},\mathbf{z})} \quad \text{s.t.} \quad (7),(8),(14),(15), \tag{59}$$

because it automatically leads to both high power efficiency (in terms of SR/power consumptions) and high rate, without enforcing the rate-fairness constraint (54b). Algorithm 3, which is similar to Algorithm 2, provides the pseudo-code for its solution. At the κ-iteration, for $\eta^{(\kappa)} \triangleq \frac{K}{\pi(w^{(\kappa)},z^{(\kappa)})}\max_{k\in\mathcal{K}} r_k(w^{(\kappa)},z^{(\kappa)})$ it iterates the problem

$$\max_{\mathbf{w}} \left[\tilde{f}_{GM,1}^{(\kappa)}(\mathbf{w}) - \eta^{(\kappa)}\pi(\mathbf{w},z^{(\kappa)})\right] \quad \text{s.t.} \quad (14),(22b). \tag{60}$$

instead of (48) to generate $w^{(\kappa+1)}$, and iterates the problem

$$\max_{\mathbf{z}} \left[\tilde{f}_{GM,2}^{(\kappa)}(\mathbf{z}) - \eta^{(\kappa)}\pi(w^{(\kappa+1)},\mathbf{z}) - \rho\sum_{m\in\mathcal{M}} |\mathbf{z}_m - p_m^{(\kappa)}e^{\jmath\theta_m^{(\kappa)}}|^2\right] \quad \text{s.t.} \quad (30b), \tag{61}$$

instead of (52) to generate $z^{(\kappa+1)}$.

Based on (47), (14), and (16), we have

$$\tilde{f}_{GM,1}^{(\kappa)}(\mathbf{w}) - \eta^{(\kappa)}\pi(\mathbf{w},z^{(\kappa)}) = a_1^{(\kappa)} + 2\sum_{k\in\mathcal{K}} \Re\{\lambda_{1,k}^{(\kappa)}\psi_{1,k}^{(\kappa)}\mathbf{w}_k\} - \sum_{k\in\mathcal{K}} \mathbf{w}_k^H\tilde{\Psi}_1^{(\kappa)}\mathbf{w}_k, \tag{62}$$

for $a_1^{(\kappa)} \triangleq \sum_{k\in\mathcal{K}} \lambda_k^{(\kappa)}a_{1,k}^{(\kappa)} - \eta^{(\kappa)}\tau_{RIS}\sigma_\nu||z^{(\kappa)}||^2 - \eta^{(\kappa)}P_{non}$, and $\tilde{\Psi}_1^{(\kappa)} \triangleq \Psi_1^{(\kappa)} + \eta^{(\kappa)}\tau_{BS}I_N + \eta^{(\kappa)}\tau_{RIS}\mathcal{Q}_1(z^{(\kappa)})$, so the problem (61) is in the form of (98) and thus it can be solved by the innovative bisection procedure described in Appendix II.

By (17) and (51)

$$\tilde{f}_{GM,2}^{(\kappa)}(\mathbf{z}) - \eta^{(\kappa)}\pi(w^{(\kappa+1)},\mathbf{z}) = a^{(\kappa)} + 2\Re\{\psi_2^{(\kappa)}\mathbf{z}\} + \mathbf{z}^H\tilde{\Psi}_2^{(\kappa)}\mathbf{z}, \tag{63}$$

for

$$a^{(\kappa)} \triangleq a_2^{(\kappa)} - \eta^{(\kappa)}\tau_{BS}\sum_{k\in\mathcal{K}} ||w_k^{(\kappa+1)}||^2 - \eta^{(\kappa)}P_{non},$$

and

$$\tilde{\Psi}_2^{(\kappa)} \triangleq \Psi_2^{(\kappa)} + \eta^{(\kappa)}\tau_{RIS}\mathcal{Q}_2(w^{(\kappa+1)}).$$

Like (52), (61) admits a closed-form solution

$$z^{(\kappa+1)} = \begin{cases} (\tilde{\Psi}_2^{(\kappa)} + \rho I_M)^{-1}\xi^{(\kappa)} \\ \text{if} \quad ||\sqrt{\mathcal{Q}_2^{(\kappa)}}(\tilde{\Psi}_2^{(\kappa)} + \rho I_M)^{-1}\xi^{(\kappa)}||^2 \leq P_A \\ (\tilde{\Psi}_2^{(\kappa)} + \rho I_M + \alpha\mathcal{Q}_2^{(\kappa)})^{-1}\xi^{(\kappa)} \quad \text{otherwise,} \end{cases} \tag{64}$$

where $\alpha > 0$ is found by bisection so that $||\sqrt{\mathcal{Q}_2^{(\kappa)}}(\tilde{\Psi}_2^{(\kappa)} + \rho I_M + \alpha\mathcal{Q}_2^{(\kappa)})^{-1}\xi^{(\kappa)}||^2 = P_A$.

Algorithm 3 QoS aware EE scalable algorithm of scalable complexity

1: **Initialization:** Randomly generate a feasible four-tuple $(w^{(0)},z^{(0)},p^{(0)},\theta^{(0)})$ for (8), (14), (15). Set $\kappa = 0$.
2: **Repeat until convergence:** Define $\lambda_k^{(\kappa)}$ by (44). Generate $w^{(\kappa+1)}$ by solving (62), $z^{(\kappa+1)}$ by (64). Generate $(p^{(\kappa+1)},\theta^{(\kappa+1)})$ by (37)-(38). Reset $\kappa \leftarrow \kappa+1$.
3: **Output** $(w^{(\kappa)},z^{(\kappa)},p^{(\kappa)},\theta^{(\kappa)})$ and $r_k(w^{(\kappa)},z^{(\kappa)})$, $k\in\mathcal{K}$.

IV. Scalable-complex soft max-min rate optimization algorithm

Note that for $c>0$, we have:

$$\max_{\mathbf{w},\mathbf{z},} \min_{k\in\mathcal{K}} r_k(\mathbf{w},\mathbf{z}) \Leftrightarrow \max_{\mathbf{w},\mathbf{z}} \left[-\max_{k\in\mathcal{K}} \ln\left(1+\frac{1}{\mu}\frac{|\tilde{\hbar}_k(\mathbf{z})\mathbf{w}_k|^2}{\varphi_k(\mathbf{w},\mathbf{z})}\right)^{-1}\right], \tag{65}$$

while

$$\max_{k\in\mathcal{K}} \ln\left(1+\frac{1}{\mu}\frac{|\tilde{\hbar}_k(\mathbf{z})\mathbf{w}_k|^2}{\varphi_k(\mathbf{w},\mathbf{z})}\right)^{-1} \leq \tag{66}$$

$$\ln\left(\sum_{k\in\mathcal{K}}\left(1+\frac{1}{\mu}\frac{|\tilde{\hbar}_k(\mathbf{z})\mathbf{w}_k|^2}{\varphi_k(\mathbf{w},\mathbf{z})}\right)^{-1}\right) \leq \tag{67}$$

$$\max_{k\in\mathcal{K}} \ln\left(1+\frac{1}{\mu}\frac{|\tilde{\hbar}_k(\mathbf{z})\mathbf{w}_k|^2}{\varphi_k(\mathbf{w},\mathbf{z})}\right)^{-1} + \ln K. \tag{68}$$

For $\mu > 0$, the constant $\ln K$ is small compared to the absolute value of the non-smooth function on the LHS of (66). Therefore the function in the LHS of (67), which is

$$f_{SM}(\mathbf{w},\mathbf{z}) = \ln\left(\sum_{k\in\mathcal{K}} \nu_k(\mathbf{w},\mathbf{z})\right) \tag{69}$$

with

$$\nu_k(\mathbf{w},\mathbf{z}) \triangleq 1 - \frac{|\tilde{\hbar}_k(\mathbf{z})\mathbf{w}_k|^2}{|\tilde{\hbar}_k(\mathbf{z})\mathbf{w}_k|^2 + \mu\varphi_k(\mathbf{w},\mathbf{z})}, \tag{70}$$

provides a good approximation for that in the LHS of (66). As such, the MR problem (19) can be addressed via the following soft min problem for small $\mu > 0$:

$$\min_{\mathbf{w},\mathbf{z}} f_{SM}(\mathbf{w},\mathbf{z}) \quad \text{s.t} \quad (7),(8),(14),(15). \tag{71}$$

Similarly to (19), the penalized optimization formulation for (71) is

$$\min_{\mathbf{w},\mathbf{z}} f_{\rho,SM}(\mathbf{w},\mathbf{z}) \quad \text{s.t} \quad (8),(14),(15), \tag{72}$$

for

$$f_{\rho,SM}(\mathbf{w},\mathbf{z}) \triangleq \left[f_{SM}(\mathbf{w},\mathbf{z}) + \rho \sum_{m\in\mathcal{M}} |\mathbf{z}_m - \boldsymbol{p}_m e^{\jmath\boldsymbol{\theta}_m}|^2 \right].$$

Initialized by feasible point $(w^{(0)}, z^{(0)}, p^{(0)}, \theta^{(0)})$ for (72), let $(w^{(\kappa)}, z^{(\kappa)}, p^{(\kappa)}, \theta^{(\kappa)})$ be a feasible point for (72) that is found from the $(\kappa-1)$-st iteration. We now provide the corresponding alternating descent in each of $\mathbf{w}$ and $\mathbf{z}$, since it is plausible that the alternating descent in $(\boldsymbol{p},\boldsymbol{\theta})$ is still based on the closed forms (37)-(38).

A. Beamforming descent

To seek $w^{(\kappa+1)}$ so that

$$\begin{aligned} & f_{\rho,SM}(w^{(\kappa+1)}, z^{(\kappa)}) < f_{\rho,SM}(w^{(\kappa)}, z^{(\kappa)}) \\ \Leftrightarrow \quad & f_{SM}(w^{(\kappa+1)}, z^{(\kappa)}) < f_{SM}(w^{(\kappa)}, z^{(\kappa)}), \end{aligned} \tag{73}$$

we consider the following problem

$$\min_{\mathbf{w}} \ f_{SM,1}^{(\kappa)}(\mathbf{w}) \quad \text{s.t.} \quad (14),(22b), \tag{74}$$

where in accordance with (23), $f_{SM,1}^{(\kappa)}(\mathbf{w}) \triangleq f_{SM}(\mathbf{w}, z^{(\kappa)}) \triangleq \ln \nu_1^{(\kappa)}(\mathbf{w})$ for

$$\nu_1^{(\kappa)}(\mathbf{w}) \triangleq \sum_{k\in\mathcal{K}} \left(1 - \frac{|h_{1,k}^{(\kappa)}\mathbf{w}_k|^2}{|h_{1,k}^{(\kappa)}\mathbf{w}_k|^2 + \mu\varphi_{1,k}^{(\kappa)}(\mathbf{w})} \right). \tag{75}$$

Using the inequality (97) for $(\mathbf{v}_k, \mathbf{y}_k) = [h_{1,k}^{(\kappa)}\mathbf{w}_k, \varphi_{1,k}^{(\kappa)}(\mathbf{w})]$, $k \in \mathcal{K}$, and $(\bar{v}_k, \bar{y}_k) = (v_{1,k}^{(\kappa)}, y_{1,k}^{(\kappa)}) \triangleq [h_{1,k}^{(\kappa)} w_k^{(\kappa)}, \varphi_{1,k}^{(\kappa)}(w^{(\kappa)})]$, yields the following tight majorant of $f_{SM}(\mathbf{w}, z^{(\kappa)})$ at $w^{(\kappa)}$:

$$\begin{aligned} f_{1,SR}^{(\kappa)}(\mathbf{w}) \ &\triangleq \ a_1^{(\kappa)} - 2\sum_{k\in\mathcal{K}} \Re\{b_{1,k}^{(\kappa)}\mathbf{w}_k\} + \sum_{k\in\mathcal{K}} c_{1,k}^{(\kappa)} (|h_{1,k}^{(\kappa)}\mathbf{w}_k|^2 \\ &\qquad + \mu \sum_{j\in\mathcal{K}\setminus\{k\}} |h_{1,k}^{(\kappa)}\mathbf{w}_j|^2) \quad (76) \\ &= a_1^{(\kappa)} - 2\sum_{k\in\mathcal{K}} \Re\{b_{1,k}^{(\kappa)}\mathbf{w}_k\} + \sum_{k\in\mathcal{K}} (\mathbf{w}_k)^H \mathcal{B}_{1,k}^{(\kappa)} \mathbf{w}_k, \quad (77) \end{aligned}$$

where

$$\begin{aligned} a_1^{(\kappa)} \ \triangleq \ & \ln \nu_1^{(\kappa)}(w^{(\kappa)}) + \frac{1}{\nu_1^{(\kappa)}(w^{(\kappa)})} \sum_{k\in\mathcal{K}} \Big(\frac{|v_{1,k}^{(\kappa)}|^2}{\mu y_{1,k}^{(\kappa)} + |v_{1,k}^{(\kappa)}|^2} \\ & + \frac{|v_{1,k}^{(\kappa)}|^2}{(\mu y_{1,k}^{(\kappa)} + |v_{1,k}^{(\kappa)}|^2)^2} \mu\sigma_{1,k}^{(\kappa)} \Big), \end{aligned} \tag{78}$$

$$\mathbb{C}^N \ni b_{1,k}^{(\kappa)} \triangleq \frac{1}{\nu_1^{(\kappa)}(w^{(\kappa)})} \frac{(v_{1,k}^{(\kappa)})^*}{\mu y_1^{(\kappa)} + |v_{1,k}^{(\kappa)}|^2} h_{1,k}^{(\kappa)}, k \in \mathcal{K}, \tag{79}$$

$$c_{1,k}^{(\kappa)} \triangleq \frac{1}{\nu_1^{(\kappa)}(w^{(\kappa)})} \frac{|v_{1,k}^{(\kappa)}|^2}{(\mu y_1^{(\kappa)} + |v_{1,k}^{(\kappa)}|^2)^2}, k \in \mathcal{K}, \tag{80}$$

and

$$\mathcal{B}_{1,k}^{(\kappa)} \triangleq c_{1,k}^{(\kappa)} (h_{1,k}^{(\kappa)})^H h_{1,k}^{(\kappa)} + \mu \sum_{j\in\mathcal{K}\setminus\{k\}} c_{1,j}^{(\kappa)} (h_{1,j}^{(\kappa)})^H h_{1,j}^{(\kappa)}, k \in \mathcal{K}. \tag{81}$$

We thus use the innovative bisection procedure of scalable complexity described in Appendix II to solve the following convex problem of majorant minimization for (74) to generate $w^{(\kappa+1)}$ verifying (73):

$$\min_{\mathbf{w}} \ f_{1,SR}^{(\kappa)}(\mathbf{w}) \quad \text{s.t.} \quad (14),(22b). \tag{82}$$

B. aRIS descent

To seek $z^{(\kappa+1)}$ so that

$$f_{\rho,SM}(w^{(\kappa+1)}, z^{(\kappa+1)}) < f_{\rho,SM}(w^{(\kappa+1)}, z^{(\kappa)}), \tag{83}$$

we consider the following problem:

$$\min_{\mathbf{z}} \ f_{\rho,SM,3} \triangleq \left[f_{SM,2}^{(\kappa)}(\mathbf{z}) + \rho \sum_{m\in\mathcal{M}} |\mathbf{z}_m - p_m^{(\kappa)} e^{\jmath\theta_m^{(\kappa)}}|^2 \right] \quad \text{s.t.} \quad (30b), \tag{84}$$

where in accordance to (31), $f_{SM,2}^{(\kappa)}(\mathbf{z}) \triangleq f_{SM}(w^{(\kappa+1)}, \mathbf{z}) = \ln \nu_2^{(\kappa)}(\mathbf{z})$, with

$$\nu_2^{(\kappa)}(\mathbf{z}) \triangleq \sum_{k\in\mathcal{K}} \left(1 - \frac{|\tau_{k,k}^{(\kappa)} + \Delta_{k,k}^{(\kappa)}\mathbf{z}|^2}{|\tau_{k,k}^{(\kappa)} + \Delta_{k,k}^{(\kappa)}\mathbf{z}|^2 + \mu\varphi_{2,k}^{(\kappa)}(\mathbf{z})} \right), k \in \mathcal{K}. \tag{85}$$

Using the inequality (97) for $(\mathbf{v}_k, \mathbf{y}_k) = [\tau_{k,k}^{(\kappa)} + \Delta_{k,k}^{(\kappa)}\mathbf{z}, \varphi_{2,k}^{(\kappa)}(\mathbf{z})]$, $k \in \mathcal{K}$ and $(\bar{v}_k, \bar{y}_k) = (v_{2,k}^{(\kappa)}, y_{2,k}^{(\kappa)}) \triangleq [\tau_{k,k}^{(\kappa)} + \Delta_{k,k}^{(\kappa)} z^{(\kappa)}, \varphi_{2,k}^{(\kappa)}(z^{(\kappa)})]$, $k \in \mathcal{K}$ yields the following tight majorant of $f_{SM,2}^{(\kappa)}(\mathbf{z})$ at $z^{(\kappa)}$:

$$\begin{aligned} \tilde{f}_{2,SM}^{(\kappa)}(\mathbf{z}) \triangleq \ & \tilde{a}_2^{(\kappa)} - 2\sum_{k\in\mathcal{K}} \Re\{d_{2,k}^{(\kappa)}(\tau_{k,k}^{(\kappa)} + \Delta_{k,k}^{(\kappa)}\mathbf{z})\} \\ & + \sum_{k\in\mathcal{K}} c_{2,k}^{(\kappa)} (|\tau_{k,k}^{(\kappa)} + \Delta_{k,k}^{(\kappa)}\mathbf{z}|^2 + \mu(\sum_{j\in\mathcal{K}\setminus\{k\}} |\tau_{k,j}^{(\kappa)} \\ & + \Delta_{k,j}^{(\kappa)}\mathbf{z}|^2 + \sigma_\nu \mathbf{z}^H \mathcal{D}_k \mathbf{z})) \quad (86) \\ = \ & a_2^{(\kappa)} - 2\Re\{b_2^{(\kappa)}\mathbf{z}\} + \mathbf{z}^H \mathcal{B}_2^{(\kappa)} \mathbf{z}, \quad (87) \end{aligned}$$

where

$$\begin{aligned} \tilde{a}_2^{(\kappa)} \ \triangleq \ & \ln \nu_2^{(\kappa)}(z^{(\kappa)}) + \frac{1}{\nu_2^{(\kappa)}(z^{(\kappa)})} \sum_{k\in\mathcal{K}} \Big(\frac{|v_{2,k}^{(\kappa)}|^2}{\mu y_{2,k}^{(\kappa)} + |v_{2,k}^{(\kappa)}|^2} \\ & + \frac{|v_{2,k}^{(\kappa)}|^2}{(\mu y_{2,k}^{(\kappa)} + |v_{2,k}^{(\kappa)}|^2)^2} \mu\sigma \Big), \end{aligned} \tag{88}$$

$$d_{2,k}^{(\kappa)} \triangleq \frac{1}{\nu_2^{(\kappa)}(z^{(\kappa)})} \frac{(v_{2,k}^{(\kappa)})^*}{\mu y_{2,k}^{(\kappa)} + |v_{2,k}^{(\kappa)}|^2}, k \in \mathcal{K}, \tag{89}$$

$$c_{1,k}^{(\kappa)} \triangleq \frac{1}{\nu_2^{(\kappa)}(z^{(\kappa)})} \frac{|v_{2,k}^{(\kappa)}|^2}{(\mu y_{2,k}^{(\kappa)} + |v_{2,k}^{(\kappa)}|^2)^2}, k \in \mathcal{K}, \tag{90}$$

in (86), and

$$a_2^{(\kappa)} \triangleq \tilde{a}_2^{(\kappa)} - 2\sum_{k\in\mathcal{K}} \Re\{d_{2,k}^{(\kappa)}\tau_{k,k}^{(\kappa)}\} + \sum_{k\in\mathcal{K}} c_{2,k}^{(\kappa)}(|\tau_{k,k}^{(\kappa)}|^2 + \mu \sum_{j\in\mathcal{K}\setminus\{k\}} |\tau_{k,j}^{(\kappa)}|^2), \quad (91)$$

$$\mathbb{C}^M \ni b_2^{(\kappa)} \triangleq \sum_{k\in\mathcal{K}} d_{2,k}^{(\kappa)}\Delta_{k,k}^{(\kappa)} - \sum_{k\in\mathcal{K}} c_{2,k}^{(\kappa)}((\tau_{k,k}^{(\kappa)})^*\Delta_{k,k}^{(\kappa)} + \mu(\sum_{j\in\mathcal{K}\setminus\{k\}} (\tau_{k,j}^{(\kappa)})^*\Delta_{k,j}^{(\kappa)})), \quad (92)$$

$$\mathcal{B}_2^{(\kappa)} \triangleq \sum_{k\in\mathcal{K}} c_{2,k}^{(\kappa)}((\Delta_{k,k}^{(\kappa)})^H\Delta_{k,k}^{(\kappa)} + \mu(\sum_{j\in\mathcal{K}\setminus\{k\}} (\Delta_{k,j}^{(\kappa)})^H\Delta_{k,j}^{(\kappa)} + \sigma_\nu\mathcal{D}_k)). \quad (93)$$

We thus solve the following convex problem of majorant minimization of (84) to generate $z^{(\kappa+1)}$ verifying (83):

$$\min_{\mathbf{z}} \left[\tilde{f}_{2,SM}^{(\kappa)}(\mathbf{z}) + \rho\sum_{m\in\mathcal{M}} |\mathbf{z}_m - p_m^{(\kappa)}e^{\jmath\theta_m^{(\kappa)}}|^2\right] \quad \text{s.t.} \quad (30b). \quad (94)$$

Like (52) and (61), (94) admits a closed-form solution

$$z^{(\kappa+1)} = \begin{cases} (\mathcal{B}_2^{(\kappa)} + \rho I_M)^{-1}\xi_2^{(\kappa)} \\ \text{if} \quad ||\sqrt{\mathcal{Q}_2^{(\kappa)}}(\mathcal{B}_2^{(\kappa)} + \rho I_M)^{-1}\xi_2^{(\kappa)}||^2 \le P_A \\ (\mathcal{B}_2^{(\kappa)} + \rho I_M + \alpha\mathcal{Q}_2^{(\kappa)})^{-1}\xi_2^{(\kappa)} \quad \text{otherwise,} \end{cases}$$

where $\xi_2^{(\kappa)} \triangleq (b_2^{(\kappa)})^H + \rho(p_1^{(\kappa)}e^{\jmath\theta_1^{(\kappa)}}, \ldots, p_M^{(\kappa)}e^{\jmath\theta_M^{(\kappa)}})^T$, and $\alpha > 0$ is found by bisection so that

$$||\sqrt{\mathcal{Q}_2^{(\kappa)}}(\mathcal{B}_2^{(\kappa)} + \rho I_M + \alpha\mathcal{Q}_2^{(\kappa)})^{-1}\xi_2^{(\kappa)}||^2 = P_A.$$

C. Convergence and computational efficiency

Algorithm 4 provides the pseudo code for solving the problem (72). It follows from (73), (83) and (39) that

$$f_{\rho,SM}(w^{(\kappa+1)}, z^{(\kappa+1)}, p^{(\kappa+1)}, \theta^{(\kappa+1)}) < f_{\rho,SM}(w^{(\kappa)}, z^{(\kappa)}, p^{(\kappa)}, \theta^{(\kappa)}), \quad (95)$$

so the sequence $\{(w^{(\kappa)}, z^{(\kappa)}, p^{(\kappa)}, \theta^{(\kappa)})\}$ of improved feasible points for (72) converges to $(\bar{w}, \bar{z}, \bar{p}, \bar{\theta})$, which is a feasible point for (71).

Algorithm 4 Scalable-complex soft max-min algorithm

1: **Initialization:** Randomly generate a feasible four-tuple $(w^{(0)}, z^{(0)}, p^{(0)}, \theta^{(0)})$ for (72). Set $\kappa = 0$.
2: **Repeat until convergence:** Generate $w^{(\kappa+1)}$ by solving (82), and $z^{(\kappa+1)}$ by (95). Generate $(p^{(\kappa+1)}, \theta^{(\kappa+1)})$ by (37)-(38). Reset $\kappa \leftarrow \kappa + 1$.
3: **Output** $(w^{(\kappa)}, z^{(\kappa)}, p^{(\kappa)}, \theta^{(\kappa)})$ and $r_k(w^{(\kappa)}, z^{(\kappa)})$, $k \in \mathcal{K}$.

V. Simulations

In (2), $h_{R,k} = \sqrt{\beta_{R,k}}\bar{h}_{R,k}$ and $G_{B,R} = \sqrt{\beta_{B,R}}\bar{G}_{B,R}$, with the path-loss and large-scale fading $\beta_{R,k} = G_{RIS} - 33.05 - 30\log_{10}(d_{R,k})$ and $\beta_{B,R} = G_{BS} + G_{RIS} - 35.9 - 22\log_{10}(d_{B,R})$ at the distances $d_{R,k}$ and $d_{B,R}$ from the RIS to user k and that from the BS to the RIS. The antenna gains are $G_{RIS} = G_{BS} = 5$ dBi, while $\bar{h}_{R,k} = \sqrt{\frac{L}{L+1}}\hat{h}_{R,k}^{LoS} + \sqrt{\frac{1}{L+1}}\hat{h}_{R,k}^{NLoS}$ follow Rician distribution with the Rician factor of $L = 4.7$ dB and the line of sight (LoS) as well as non-LoS (NLoS) components of $\hat{h}_{R,k}^{LoS}$ and $\hat{h}_{R,k}^{NLoS}$, where $\bar{G}_{B,R}$ is the small scale Rician fading [5], [36], [37]. In (3), $h_k = \sqrt{\beta_k}\bar{h}_k$ with the path-loss and large-scale fading $\sqrt{\beta_k} = G_{\text{BS}} - 33.05 - 36.7\log_{10}(d_{\text{k}})$ at the distance d_{k} from the BS to user k. The small-scale fading channel gain $\bar{h}_k$ of the BS to user k obeys the Rayleigh distribution [6]. Furthermore, the values of small scale fading $\bar{G}_{B,R}$ are generated by $\bar{G}_{B,R}(m,n) = e^{\jmath\pi\left((m_1-1)\sin\bar{\theta}_m\sin\bar{\psi}_m + (n-1)\sin e^{\jmath\theta_m}\sin\psi_m\right)}$, with $e^{\jmath\theta_m}$ and ψ_m following uniform distribution within $(0,\pi)$ and $(0,2\pi)$, respectively. Furthermore, we set $\bar{\theta}_m = \pi - \theta_m$ and $\bar{\phi}_m = \pi + \phi_m$ [37]. The noise power density is set to -174 dBm/Hz.

The 3-D coordinates of the BS and RIS in Fig. 2 are set to $(120, 0, 25)$ m and $(0, 90, 40)$ m, where the total $K = 8$ users are randomly located in two circular areas centered at $(0, 90, 40)$ m and $(240, 90, 40)$m with the radius of 60m.

Unless specified otherwise, we assume that the number of antennas is $N = 8$, the transmit power is $P = 20$dBm, the number of RIS elements is $M = 100$ and the power split between the BS and RIS is $0.99P$ and $0.01P$.

The following legends are used to specify the proposed implementations: (i) MR RIS refers to the performance of the CQ-based Algorithm 1 designed for solving the MR problem (20); (ii) GM-RIS and SR-RIS (GM w/o RIS and SR w/o RIS, resp.) refer to the performance of the scalable Algorithm 2 conceived for solving the GM-rate problem (42) and SR problem (53) (w/o, resp.); (iii) soft MR-RIS (soft MR w/o RIS, resp.) refers to the performance of the scalable Algorithm 4 of RIS-assisted signaling (RIS-less signaling, resp.).

A. Algorithmic convergence and efficiency

The choice of the penalty parameter μ in equations (20), (42) and (72) is of paramount importance for the algorithms' convergence. Starting with an initial value of $\mu = 1e^{-3}$, we amplify it by a factor of 1.2 in each iteration. As the iterative procedure unfolds, the value of μ gradually increases, eventually resulting in the converge of the objective function and the subsequent reduction of the penalty term to zero.

Similarly, the choice of c in soft max-min problem (72) is also significant as a smaller value of c does not necessarily translate to improved MR performance. This is evident from Table II, which presents the achieved MR versus $c \in \{1, 0.5, 0.1\}$ under different number of BS antennas N. For $N \in \{6, 7\}$, soft-MR RIS with $c = 1$ yields the lowest MR, while soft-MR RIS with $c = 0.1$ and $c = 0.5$ exhibit similar MR. In the case of $N \in \{8, 9, 10\}$, soft-MR RIS with $c = 1$ demonstrates the MR is quite similar to that with

$c = 0.5$. Therefore, $c = 0.5$ emerges as the magic choice for achieving consistent performance.

Fig. 3(a) and Fig. 3(b) depict convergence patterns of the objective functions and the penalty terms toward zero. In particular, as shown in Fig. 3(a) the objective functions of the MR RIS and GM RIS (soft min, resp.) increased (decreased, resp.) rapidly within 10-20 iterations, followed by a gradual convergence. Similarly, Fig. 3(b) shows that the penalty terms practically converge to zero within the same range of iterations.

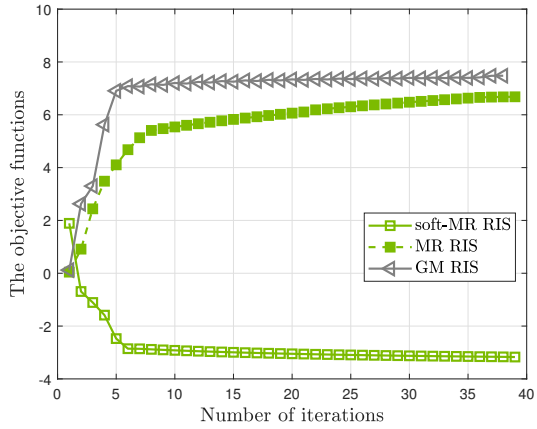

(a)

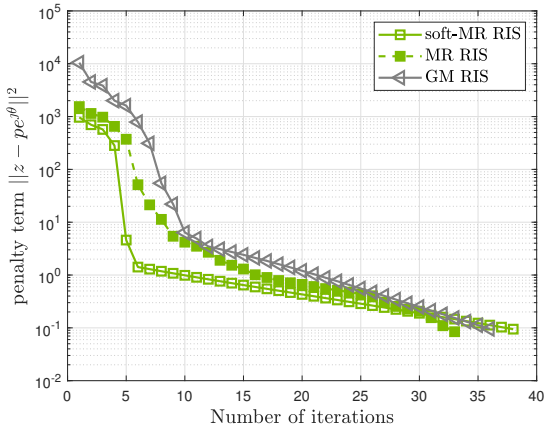

(b)

Fig. 3: The convergence of the proposed algorithms

B. Achievable MR and SR by aRIS-aided signaling

Fig. 4(a) and Fig. 4(b) depict the MR and SR versus the number of BS antennas N achieved by the proposed algorithms. Surprisingly, the MR of soft-MR RIS is even slightly better than that of MR RIS in Fig. 4(a). As expected, the SR achieved by soft-MR RIS is much better than that attained by MR RIS in Fig. 4(b). Note that the soft-MR RIS relies on closed-form expressions of scalable computational complexity, while MR RIS is optimized by CQ of cubic computational complexity. Hence the former is better than the latter in terms of its performance versus complexity. We thus safely depart from MR RIS from now on.

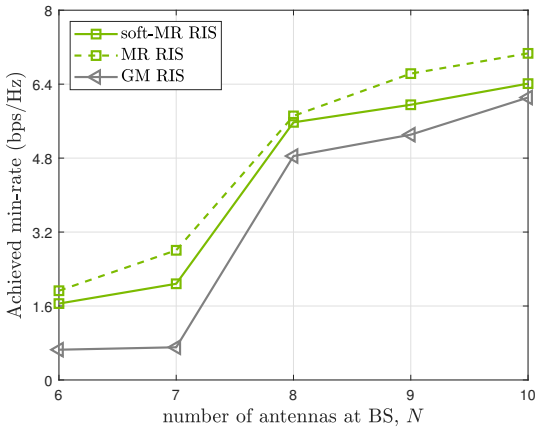

(a)

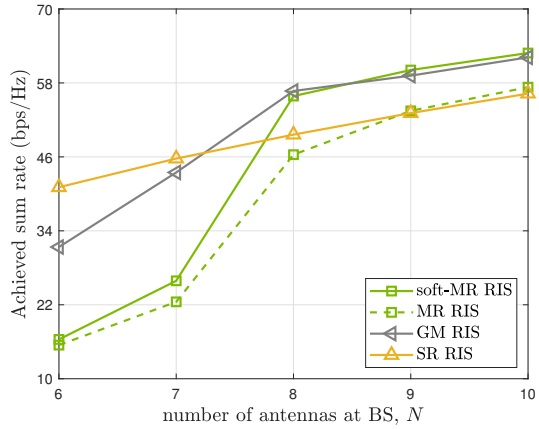

(b)

Fig. 4: The min-rate and sum rate versus the number of BS antennas N achieved by the proposed algorithms.

Table III provides the average number of zero-rate users (ZR-UEs) for SR maximization, demonstrating that the zero rate problem is an inherent issue. Hence the stand-alone SR maximization is unsuitable for MU communications.

C. aRIS vs no RIS

Fig. 5(a) and Fig. 5(b), which plot the MR and SR achieved clearly show the performance advantage of an aRIS-assisted solution which increases with the number of BS antennas N. The MR achieved by the soft-MR RIS is better than that of GM RIS. In terms of SR, soft-MR RIS is outperformed by GM RIS for $N < 8$, but the former catches up for $N \geq 8$. It is worth mentioning that both GM RIS and soft-MR RIS achieve a better SR than that of the stand-alone SR maximization, when $N > K$.

Fig. 6(a) and Fig. 6(b), which depict the rate distributions of the proposed algorithms, show that both the soft-MR and GM algorithms exhibit a fair MU rate distribution. All users' rates are reasonably similar.

TABLE II: The achieved MR versus c under different number of BS antennas N by soft-MR maximization.

	N = 6	N = 7	N = 8	N = 9	N = 10
c = 0.1 soft-MR RIS	1.6517	2.2011	4.9702	5.3726	5.7722
c = 0.5 soft-MR RIS	1.6378	2.1413	5.2849	5.8613	6.2480
c = 1 soft-MR RIS	0.5972	1.2214	5.2987	5.8900	6.2929

TABLE III: The average number of ZR-UEs versus the number of BS antennas N by SR maximization

	M = 6	M = 7	M = 8	M = 9	M = 10
SR RIS	2.33	1.90	1.40	0.97	0.87
SR w/o RIS	2.80	2.50	1.83	1.43	1.33

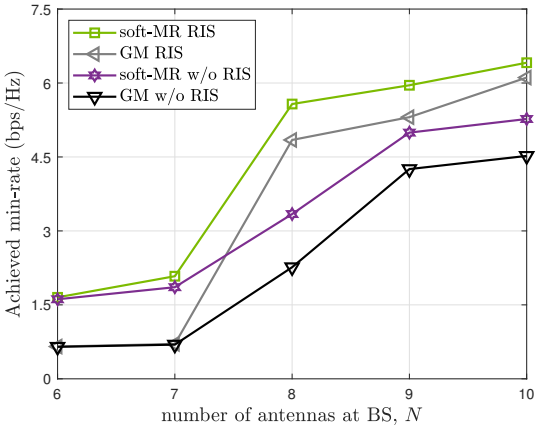

(a)

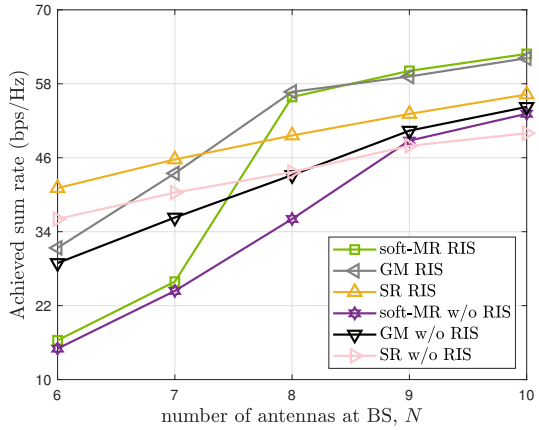

(b)

Fig. 5: The min-rate and sum rate achieved versus the number of BS antennas N.

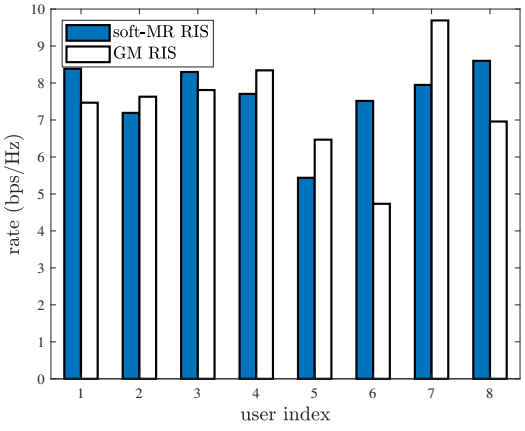

(a)

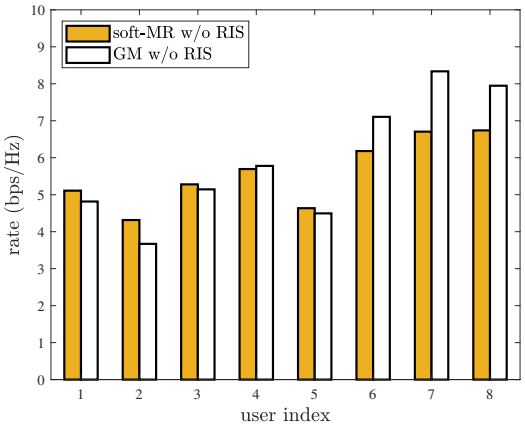

(b)

Fig. 6: Rate distribution versus user index.

Fig. 7(a) and Fig. 7(b) show that both the MR and SR achieved increase in line with the transmit power budget P. Fig. 7 reveals that soft-MR RIS achieves a better MR than GM RIS and the SR achieved by the former gets closer to that achieved by the latter.

Furthermore, Fig. 8 shows that the MR achieved by soft-MR and GM RIS increases in line with the number of PREs. Apparently, ones have to substantially increase the number of PREs to achieve a modest improvement MR.

D. EE efficiency

For implementing (55), we set $(\tau_{BS}, \tau_{RIS}) = (0.9^{-1}, 0.8^{-1})$, while $P_{non} = NP_{a,BS} + P_{c,BS} + M(P_{a,pre} + P_{c,pre})$, where we have $(P_{a,BS}, P_{a,pre}) = (30, -10)$ dBm, which represent the circuit powers per BS antenna and RIS PRE. Furthermore, we set $(P_{c,BS}, P_{c,pre}) = (40, -5)$ dBm, which are non-transmission power at BS and RIS.

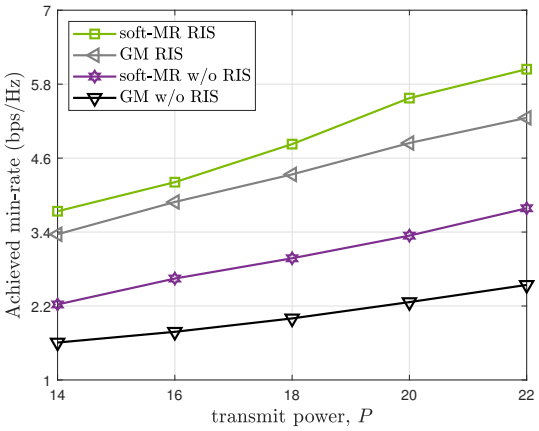

(a)

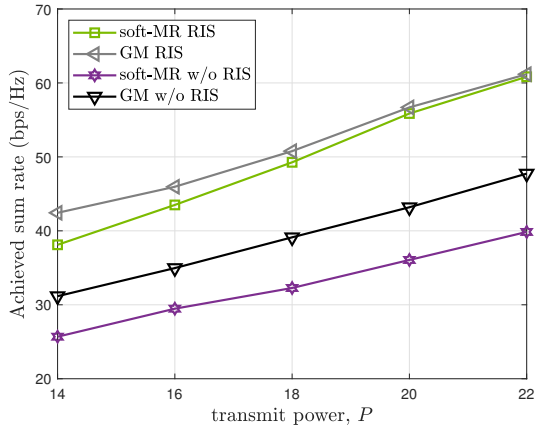

(b)

Fig. 7: The min-rate and sum rate achieved versus the transmit power P.

Fig. 9 plots the EE and MR achieved versus the number of RIS elements, M, with $N = 8$ BS-antennas and $P = 27$ dBm. Both the EE and MR are seen to be increased in line with M, and the aRIS-EE achieves substantially better EE and MR than that of its RIS-less counterpart.

E. Power split

Fig. 10 shows that both GM RIS and soft-MR achieve only slightly improved MR upon allocating more power to the aRIS.

F. Performance vs resolution

Finally, Fig. 11(a) and Fig. 11(b) show the sensitivity of the MR and SR versus the PRE resolution.

VI. Conclusions

To enhance the rate-fairness of multiple users offered by aRIS-assisted signaling, we have proposed different optimization formulations and their computational solutions. The aRISs rely on low-resolution PREs for practical implementation. We set out from the standard problem of maximizing the MR, which has been addressed by CQ-based iterations of cubic

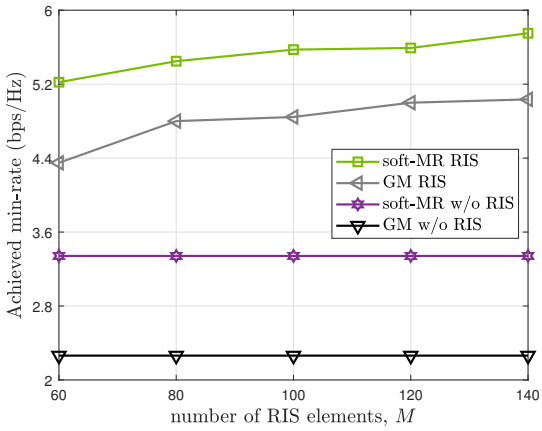

Fig. 8: The min-rate versus the number of RIS elements M achieved .

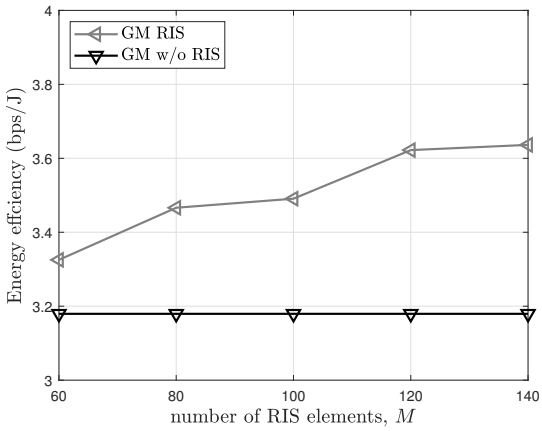

(a)

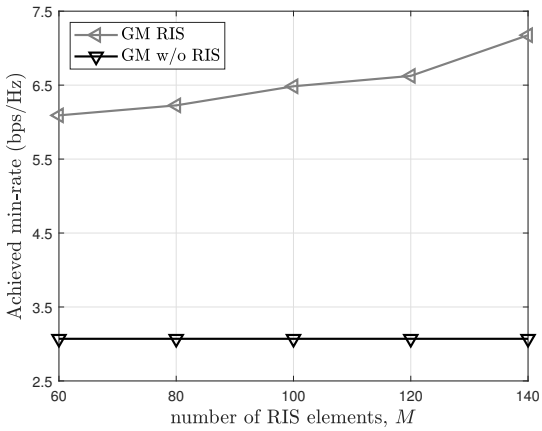

(b)

Fig. 9: The EE and min-rate versus the number of RIS elements M achieved.

computational complexity that may become excessive. Then we have proposed a pair of surrogate problems, namely that of GM-rate and soft max-min rate optimization. These achieved

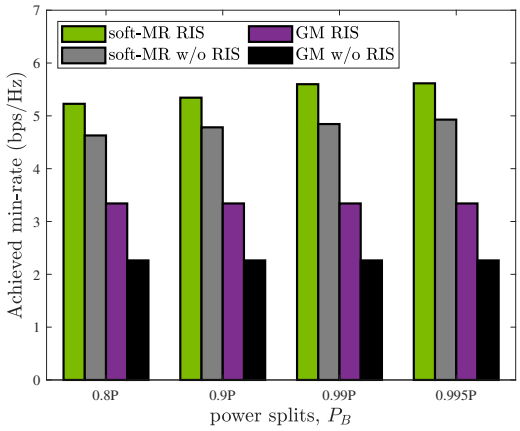

Fig. 10: The min-rate of different power splits, P_B.

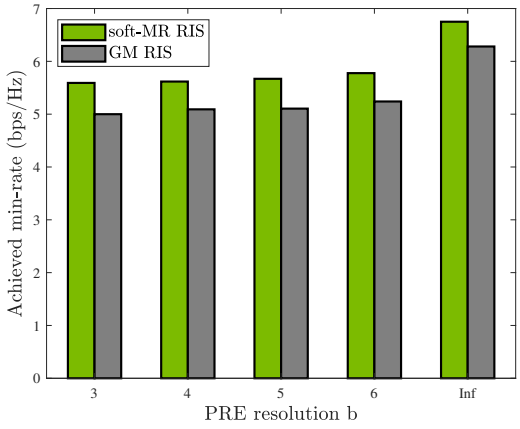

(a)

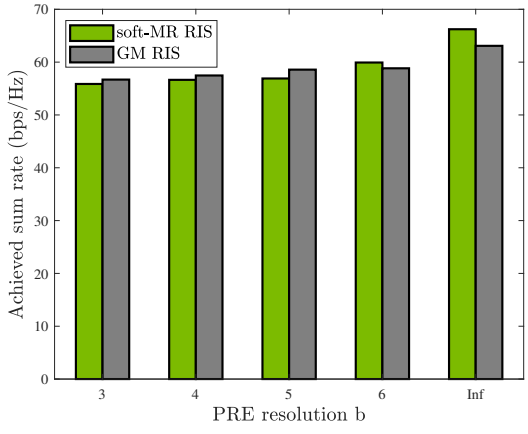

(b)

Fig. 11: The min-rate and sum rate achieved versus the reflection coefficient resolution b.

both a high MR and high sum rate, while iterating by evaluating closed-form expressions of scalable complexity. Finally, simulations have been provided to confirm their practical benefits.

Appendix I: Fundamental tight minorants and majorants

A function $\bar{f}$ is said to be a tight minorant of a function f at $\bar{v}$ over the domain $\mathrm{dom}(f)$, if $f(x) \geq \bar{f}(x)\ \forall\ x \in \mathrm{dom}(f)$ and $f(\bar{v}) = \bar{f}(\bar{v})$ [25, p. 366]. Then it can be shown that $f(\bar{v}_{opt}) > f(\bar{v})$ as far as $\bar{f}(\bar{v}_{opt}) \neq \bar{f}(\bar{v})$ for $\bar{v}_{opt} = \arg\min_{x \in \mathrm{dom}(f)} \bar{f}(x)$, i.e. a tight minorant maximization at the point $\bar{v}$ helps to obtain a better point than itself.
Analogously, a function $\bar{f}$ is said to be a tight majorant of a function f at $\bar{v}$ over the domain $\mathrm{dom}(f)$ if $f(x) \leq \bar{f}(x)\ \forall\ x \in \mathrm{dom}(f)$ and $f(\bar{v}) = \bar{f}(\bar{v})$ [25, p. 366]. Then it can be readily shown that $f(\bar{v}_{opt}) < f(\bar{v})$ as far as $\bar{f}(\bar{v}_{opt}) \neq \bar{f}(\bar{v})$ for $\bar{v}_{opt} = \arg\max_{x \in \mathrm{dom}(f)} \bar{f}(x)$, i.e. a tight minorant maximization at the point $\bar{v}$ helps to obtain a better point than itself.

The linearized function of a concave (convex, resp.) function f at $\bar{v}$ is its tight minorant (majorant, resp.) at $\bar{v}$.

The following inequality holds true for all $(\mathbf{v}, \bar{v}) \in \mathbb{C} \times \mathbb{C}$ and $\mathbf{y} > 0$, $\bar{y} > 0$ [31]:

$$\ln(1 + \frac{|\mathbf{v}|^2}{\mathbf{y}}) \ \geq\ \ln(1+\frac{|\bar{v}|^2}{\bar{y}}) - \frac{|\bar{v}|^2}{\bar{y}} + \frac{2}{\bar{y}}\Re\{\bar{v}^*\mathbf{v}\} - \frac{|\bar{v}|^2}{\bar{y}(|\bar{v}|^2 + \bar{y})}(|\mathbf{v}|^2 + \mathbf{y}), \tag{96}$$

i.e the right hand side (RHS) of (96) provides a tight minorant of the left hand side (LHS) at $(\bar{v}, \bar{y})$ over the domain $\{(\mathbf{v}, \mathbf{y}) : \mathbf{v} \in \mathbb{C}, \mathbf{y} > 0\}$.

The inequality (97) holds true for all $\mathbf{v}_k \in \mathbb{C}$, $\bar{v}_k \in \mathbb{C}$, and $\mathbf{y}_k > 0$, $\bar{y}_k > 0$, $k \in \mathcal{K}$, and $\mu > 0$, i.e. the RHS of (97) provides a tight majorant of the LHS at $(\bar{v}, \bar{y})$ over the domain $\{(\mathbf{v}_k, \mathbf{y}_k) : \mathbf{v}_k \in \mathbb{C}, \mathbf{y}_k > 0, k \in \mathcal{K}\}$. Considering the LHS as a function $f(\mathbf{v}, \mathbf{z})$ with $\mathbf{z}_k \triangleq |\mathbf{v}_k|^2 + \mu\mathbf{y}_k$, which is concave [31], the RHS is its linearized function at $(\bar{v}, \bar{z})$ with $\bar{z}_k = |\bar{v}_k|^2 + \mu\bar{y}_k$.

Appendix II: Closed-form based algorithm for two convex constrained optimization

We consider the following convex problems

$$\min_{\mathbf{v}_k \in \mathbb{C}^N, k \in \mathcal{K}} -2\sum_{k\in\mathcal{K}} \Re\{b_k^H \mathbf{v}_k\} + \sum_{k\in\mathcal{K}} \mathbf{v}_k^H \mathcal{Q}_{1,k} \mathbf{v}_k$$
$$\text{s.t.} \quad \sum_{k\in\mathcal{K}} ||\mathbf{v}_k||^2 \leq P_1, \sum_{k\in\mathcal{K}} \mathbf{v}_k^H \mathcal{Q}_{2,k} \mathbf{v}_k \leq P_2, \tag{98}$$

with given positive semi-definite matrices $\mathcal{Q}_{1,k}$ and $\mathcal{Q}_{2,k}$ and $b_k \in \mathbb{C}^N$, $k \in \mathcal{K}$, and$P_1 > 0$ and $P_2 > 0$.

Then it is plausible that the solution of (98) is

$$v_k^{opt} = \mathcal{Q}_{1,k}^{-1} b_k, l \in \mathcal{K}, \tag{99}$$

whenever

$$\sum_{k\in\mathcal{K}} ||\mathcal{Q}_{1,k}^{-1} b_k||^2 \leq P_1 \tag{100}$$

and

$$\sum_{k\in\mathcal{K}} ||\sqrt{\mathcal{Q}_{2,k}}\mathcal{Q}_{1,k}^{-1} b_k||^2 \leq P_2. \tag{101}$$

When (101) is not met, we use bisection to find μ_2 so that

$$\sum_{k\in\mathcal{K}} ||\sqrt{\mathcal{Q}_{2,k}}(\mathcal{Q}_{1,k} + \mu_2\mathcal{Q}_{2,k})^{-1} b_k||^2 = P_2. \tag{102}$$

$$\ln\left(\sum_{k\in\mathcal{K}}(1-\frac{|\mathbf{v}_k|^2}{|\mathbf{v}_k|^2+\mu\mathbf{y}_k})\right) \leq$$
$$\ln\left(\sum_{k\in\mathcal{K}}(1-\frac{|\bar{v}_k|^2}{|\bar{v}_k|^2+\mu\bar{y}_k})\right)+\left(\sum_{k\in\mathcal{K}}(1-\frac{|\bar{v}_k|^2}{|\bar{v}_k|^2+\mu\bar{y}_k})\right)^{-1}\sum_{k\in\mathcal{K}}\frac{|\bar{v}_k|^2}{|\bar{v}_k|^2+\mu\bar{y}_k}$$
$$-\left(\sum_{k\in\mathcal{K}}(1-\frac{|\bar{v}_k|^2}{|\bar{v}_k|^2+\mu\bar{y}_k}))\right)^{-1}\sum_{k\in\mathcal{K}}\left(2\frac{\Re\{\bar{v}_k^H\mathbf{v}_k\}}{|\bar{v}_k|^2+\mu\bar{y}_k})-\frac{|\bar{v}_k|^2}{(|\bar{v}_k|^2+\mu\bar{y}_k)^2}(|\mathbf{v}_k|^2+\mu\mathbf{y}_k)\right), \quad (97)$$

The solution of (98) is

$$v_k^{opt}=(\mathcal{Q}_{1,k}+\mu_2\mathcal{Q}_{2,k})^{-1}b_k, k\in\mathcal{K}, \quad (103)$$

if

$$\sum_{k\in\mathcal{K}}||(\mathcal{Q}_{1,k}+\mu_2\mathcal{Q}_{2,k})^{-1}b||^2\leq P_1. \quad (104)$$

If (100) is not met, we use bisection to find μ_1 so that

$$\sum_{k\in\mathcal{K}}||(\mathcal{Q}_{1,k}+\mu_1 I_N)^{-1}b_k||^2=P_1. \quad (105)$$

The solution of (98) is

$$v_k^{opt}=(\mathcal{Q}_{1,k}+\mu_1 I_N)^{-1}b_k, k\in\mathcal{K} \quad (106)$$

if

$$\sum_{k\in\mathcal{K}}||\sqrt{\mathcal{Q}_{2,k}}(\mathcal{Q}_{1,k}+\mu_1 I)^{-1}b_k||^2\leq P_2. \quad (107)$$

Thus, the remaining case is

$$v_k^{opt}=(\mathcal{Q}_{1,k}+\mu_1 I+\mu_2\mathcal{Q}_{2,k})^{-1}b_k, k\in\mathcal{K}, \quad (108)$$

where $\mu_1>0$ and $\mu_2>0$ are a pair of Lagrangian multipliers, so that

$$\sum_{k\in\mathcal{K}}||(\mathcal{Q}_{1,k}+\mu_1 I_N+\mu_2\mathcal{Q}_{2,k})^{-1}b_k||^2=P_1$$
$$\&\sum_{k\in\mathcal{K}}||\sqrt{\mathcal{Q}_{2,k}}(\mathcal{Q}_{1,k}+\mu_1 I_N+\mu_2\mathcal{Q}_{2,k})^{-1}b||^2=P_2, \quad (109)$$

which however are computationally intractable. We propose the so-called partial Lagrangian multiplier method, which aims to find μ_2, so that the solution v_k^{opt} of the problem

$$\min_{\mathbf{v}_k,k\in\mathcal{K}}\left[-2\sum_{k\in\mathcal{K}}\Re\{b_k^H\mathbf{v}_k\}+\sum_{k\in\mathcal{K}}\mathbf{v}_k^H\mathcal{Q}_{1,k}\mathbf{v}_k\right.$$
$$\left.+\mu_2\left(\sum_{k\in\mathcal{K}}\mathbf{v}_k^H\mathcal{Q}_{2,k}\mathbf{v}_k-P_2\right)\right] \quad \text{s.t.} \quad \sum_{k\in\mathcal{K}}||\mathbf{v}_k||^2\leq P_1, \quad (110)$$

satisfies $\sum_{k\in\mathcal{K}}||\sqrt{\mathcal{Q}_{2,k}}v_k^{opt}||^2=P_2$. For fixed μ_2, the solution of (110) is given by

$$v_k(\mu_2)=\begin{cases}(\mathcal{Q}_{1,k}+\mu_2\mathcal{Q}_{2,k})^{-1}b\\ \text{if} \quad \sum_{k\in\mathcal{K}}||(\mathcal{Q}_{1,k}+\mu_2\mathcal{Q}_{2,k})^{-1}b_k||^2\leq P_1\\ (\mathcal{Q}_{1,k}+\mu_2\mathcal{Q}_{2,k}+\mu_1 I_N)^{-1}b_k \quad \text{otherwise},\end{cases}$$

where μ_1 is found by bisection so that $\sum_{k\in\mathcal{K}}||(\mathcal{Q}_{1,k}+\mu_2\mathcal{Q}_{2,k}+\mu_1 I_N)^{-1}b_k||^2=P_1$. It follows from (107) that $\sum_{k\in\mathcal{K}}v_k^H(0)\mathcal{Q}_{2,k}v_k(0)>P_2$, while for a sufficient large μ_2, we have $\sum_{k\in\mathcal{K}}v^H(\mu_2)\mathcal{Q}_{2,k}v_k(\mu_2)<P_2$. We thus start from $\mu_l=0$ and μ_u is such that $\sum_{k\in\mathcal{K}}v_k^H(\mu_u)\mathcal{Q}_{2,k}$ $v_k(\mu_u)<P_2$ and carry out the following bisection.

Innovative bisection procedure. Set $\mu_2=(\mu_u+\mu_l)/2$ and generate $v_k(\mu_2)$ by (110). Stop the procedure if $\sum_{k\in\mathcal{K}}v_k^H(\mu_2)\mathcal{Q}_{2,k}v_k(\mu_2)\approx P_2$. Otherwise, update $\mu_l\leftarrow\mu_2$ if $\sum_{k\in\mathcal{K}}v_k^H(\mu_2)\mathcal{Q}_{2,k}v_k(\mu_2)>P_2$ or $\mu_u\leftarrow\mu_2$ if $\sum_{k\in\mathcal{K}}v_k^H(\mu_2)\mathcal{Q}_{2,k}v_k(\mu_2)<P_2$.

REFERENCES

[1] C. Pan, H. Ren, K. Wang, J. F. Kolb, M. Elkashlan, M. Chen, M. Di Renzo, Y. Hao, J. Wang, A. L. Swindlehurst, X. You, and L. Hanzo, "Reconfigurable intelligent surfaces for 6G systems: Principles, applications, and research directions," *IEEE Commun. Mag.*, vol. 59, no. 6, pp. 14–20, 2021.

[2] H. Zhang, B. Di, K. Bian, Z. Han, H. V. Poor, and L. Song, "Toward ubiquitous sensing and localization with reconfigurable intelligent surfaces," *Proc. IEEE*, vol. 110, pp. 1401–1422, Sept. 2022.

[3] C. Huang, S. Hu, G. C. Alexandropoulos, A. Zappone, C. Yuen, R. Zhang, M. D. Renzo, and M. Debbah, "Holographic MIMO surfaces for 6G wireless networks: Opportunities, challenges, and trends," *IEEE Wirel. Commun.*, vol. 27, pp. 118–125, May 2020.

[4] F. Liu, D.-H. Kwon, and S. Tretyakov, "Reflectarrays and metasurface reflectors as diffraction gratings: A tutorial," *IEEE Antenn. Propag. Mag. (early access)*, 2023.

[5] O. Ozdogan, E. Bjornson, and E. G. Larsson, "Intelligent reflecting surfaces: Physics, propagation, and pathloss modeling," *IEEE Wirel. Commun. Lett.*, vol. 9, no. 5, pp. 581–585, 2020.

[6] H. Yu, H. D. Tuan, A. A. Nasir, T. Q. Duong, and H. V. Poor, "Joint design of reconfigurable intelligent surfaces and transmit beamforming under proper and improper Gaussian signaling," *IEEE J. Sel. Areas Commun.*, vol. 38, no. 11, pp. 2589–2603, 2020.

[7] H. Yu, H. D. Tuan, E. Dutkiewicz, H. V. Poor, and L. Hanzo, "Maximizing the geometric mean of user-rates to improve rate-fairness: Proper vs. improper Gaussian signaling," *IEEE Trans. Wirel. Commun.*, vol. 21, no. 1, pp. 295–309, 2022.

[8] A. A. Nasir, H. D. Tuan, E. Dutkiewicz, H. V. Poor, and L. Hanzo, "Low-resolution RIS-aided multiuser MIMO signaling," *IEEE Trans. Commun.*, vol. 70, no. 10, pp. 6517–6531, 2022.

[9] R. Long, Y.-C. Liang, Y. Pei, and E. G. Larsson, "Active reconfigurable intelligent surface-aided wireless communications," *IEEE Trans. Wirel. Commun.*, vol. 20, pp. 4962–4975, Aug. 2021.

[10] Z. Zhang, L. Dai, X. Chen, C. Liu, F. Yang, R. Schober, and H. V. Poor, "Active RIS vs. passive RIS: Which will prevail in 6G?," *IEEE Trans. Commun.*, vol. 71, pp. 1707–1725, Mar. 2023.

[11] M. Rihan, E. Grossi, L. Venturino, and S. Buzzi, "Spatial diversity in radar detection via active reconfigurable intelligent surfaces," *IEEE Signal Process. Lett.*, vol. 29, pp. 1242–1246, 2022.

[12] L. Wu *et al.*, "A wideband amplifying reconfigurable intelligent surface," *IEEE Trans. Antenn. Prop.*, vol. 70, pp. 10623–1063, Nov. 2022.

[13] Q. Zhu, M. Li, R. Liu, Y. Liu, and Q. Liu, "Joint beamforming designs for active reconfigurable intelligent surface: A sub-connected array architecture",," *IEEE Trans. Commun.*, vol. 70, pp. 7628–7643, Nov. 2022.

[14] Y. Ma, M. Li, Y. Liu, Q. Wu, and Q. Liu, "Active reconfigurable intelligent surface for energy efficiency in MU-MISO systems," *IEEE Trans. Veh. Techn.*, vol. 72, pp. 4103–4107, Mar. 2023.

[15] H. Niu *et al.*, "Active RIS assisted rate-splitting multiple access network: Spectral and energy efficiency tradeoff," *IEEE J. Sel. Areas Commun.*, vol. 41, pp. 1452–1467, May 2023.

[16] Y. Ge and J. Fan, "Active reconfigurable intelligent surface assisted secure and robust cooperative beamforming for cognitive satellite-terrestrial networks," *IEEE Trans. Veh. Tech.*, vol. 72, pp. 4108–4113, Mar. 2023.

[17] G. Chen *et al.*, "Active IRS aided multiple access for energy-constrained IoT systems," *IEEE Trans. Wirel. Commun.*, vol. 22, pp. 1677–1694, Mar. 2023.

[18] H. H. Kha, H. D. Tuan, and H. H. Nguyen, "Joint optimization of source power allocation and cooperative beamforming for SC-FDMA multi-user multi-relay networks," *IEEE Trans. Commun.*, vol. 61, Jun. 2013.

[19] U. Rashid, H. D. Tuan, and H. H. Nguyen, "Relay beamforming designs in multi-user wireless relay networks based on throughput maximin optimization," *IEEE Trans. Commun.*, vol. 61, pp. 1739–1749, May 2013.

[20] U. Rashid, H. D. Tuan, H. H. Kha, and H. H. Nguyen, "Joint optimization of source precoding and relay beamforming in wireless MIMO relay networks," *IEEE Trans. Commun.*, vol. 62, pp. 488–499, Feb. 2014.

[21] H. H. M. Tam, H. D. Tuan, A. A. Nasir, T. Q. Duong, and H. V. Poor, "MIMO energy harvesting in full-duplex multi-user networks," *IEEE Trans. Wirel. Commun.*, vol. 16, pp. 3282–3297, May 2017.

[22] A. A. Nasir, H. D. Tuan, T. Q. Duong, and H. V. Poor, "Secure and energy-efficient beamforming for simultaneous information and energy transfer," *IEEE Trans. Wirel. Commun.*, vol. 16, pp. 7523–7537, Nov. 2017.

[23] Z. Sheng, H. D. Tuan, T. Q. Duong, and H. V. Poor, "Joint power allocation and beamforming for energy-efficient two-way multi-relay communications," *IEEE Trans.Wirel. Comm.*, vol. 16, pp. 6660–6671, Oct. 2017.

[24] W. Zhu, H. D. Tuan, E. Dutkiewicz, Y. Fang, and L. Hanzo, "Low-complexity Pareto-optimal 3D beamforming for the full-dimensional multi-user massive MIMO downlink," *IEEE Trans. Veh. Techn.*, vol. 72, pp. 8869–8885, Jul. 2023.

[25] H. Tuy, *Convex Analysis and Global Optimization (second edition)*. Springer International, 2017.

[26] Q. Wu and R. Zhang, "Intelligent reflecting surface enhanced wireless network via joint active and passive beamforming," *IEEE Trans. Wirel. Commun.*, vol. 18, pp. 5394–5409, Nov 2019.

[27] C. Huang, A. Zappone, G. C. Alexandropoulos, M. Debbah, and C. Yuen, "Reconfigurable intelligent surfaces for energy efficiency in wireless communication," *IEEE Trans. Wirel. Commun.*, vol. 18, pp. 4157–4170, Aug. 2019.

[28] L. Wei, C. Huang, G. C. Alexandropoulos, C. Yuen, Z. Zhang, and M. Debbah, "Channel estimation for ris-empowered multi-user miso wireless communications," *IEEE Trans. Commun.*, vol. 69, no. 6, pp. 4144–4157, 2021.

[29] C. Xu et al., "Channel estimation for reconfigurable intelligent surface assisted high-mobility wireless systems," *IEEE Trans. Veh. Techn.*, vol. 72, pp. 718–734, Jan. 2023.

[30] A. H. Phan, H. D. Tuan, H. H. Kha, and D. T. Ngo, "Nonsmooth optimization for efficient beamforming in cognitive radio multicast transmission," *IEEE Trans. Signal Process.*, vol. 60, pp. 2941–2951, Jun. 2012.

[31] H. H. M. Tam, H. D. Tuan, and D. T. Ngo, "Successive convex quadratic programming for quality-of-service management in full-duplex MU-MIMO multicell networks," *IEEE Trans. Commun.*, vol. 64, pp. 2340–2353, June 2016.

[32] L. D. Nguyen, H. D. Tuan, T. Q. Duong, H. V. Poor, and L. Hanzo, "Energy-efficient multi-cell massive MIMO subject to minimum user-rate constraints," *IEEE Trans. Commun.*, vol. 69, pp. 914–928, Feb. 2021.

[33] A. A. Nasir, H. D. Tuan, D. T. Ngo, T. Q. Duong, and H. V. Poor, "Beamforming design for wireless information and power transfer systems: Receive power-splitting versus transmit time-switching," *IEEE Trans. Commun.*, vol. 65, pp. 876–889, Feb. 2017.

[34] L. D. Nguyen, H. D. Tuan, T. Q. Duong, O. A. Dobre, and H. V. Poor, "Downlink beamforming for energy-efficient heterogeneous networks with massive MIMO and small cells," *IEEE Trans. Wirel. Commun.*, vol. 17, pp. 3386–3400, May 2018.

[35] H. D. Tuan, A. A. Nasir, H. Q. Ngo, E. Dutkiewicz, and H. V. Poor, "Scalable user rate and energy-efficiency optimization in cell-free massive MIMO," *IEEE Trans. Commun.*, vol. 70, pp. 6050–6065, Sept. 2022.

[36] E. Bjornson, O. Ozdogan, and E. G. Larsson, "Intelligent reflecting surface versus decode-and-forward: How large surfaces are needed to beat relaying?," *IEEE Wirel. Commun. Lett.*, vol. 9, no. 2, pp. 244–248, 2020.

[37] Q. U. A. Nadeem, A. Kammoun, A. Chaaban, M. Debbah, and M. S. Alouini, "Asymptotic max-min SINR analysis of reconfigurable intelligent surface assisted MISO systems," *IEEE Trans. Wirel. Commun.*, vol. 19, no. 12, pp. 7748–7764, 2020.

Yufeng Chen received the B.S. degree in communication engineering from Ludong University, China, in 2021. She is currently pursuing the M.S. degree with the School of information and electrical engineering, Shanghai University, Shanghai, China. Her current research interests include optimization methods for wireless communication and signal processing.

Hoang Duong Tuan received the Diploma (with Hons.) and Ph.D. degrees in applied mathematics from Odessa State University, Odesa, Ukraine, in 1987 and 1991, respectively. From 1994 to 1999, he spent nine academic years in Japan as an Assistant Professor with the Department of Electronic-Mechanical Engineering, Nagoya University, Nagoya, Japan, and from 1999 to 2003, he was an Associate Professor with the Department of Electrical and Computer Engineering, Toyota Technological Institute, Nagoya, Japan. From 2003 to 2011, he was a Professor with the School of Electrical Engineering and Telecommunications, University of New South Wales, Sydney, NSW, Australia. He is currently a Professor with the School of Electrical and Data Engineering, University of Technology Sydney, Ultimo, NSW, Australia. He has been involved in research with the areas of optimization, control, signal processing, wireless communication, and biomedical engineering for more than 25 years.

Yong Fang received the Ph.D. degree in electronic engineering from the City University of Hong Kong, Hong Kong, in 1999. He is currently a Professor with the School of Communication and Information Engineering, Shanghai University, Shanghai, China. His research interests include communication signal processing, blind signal processing, and adaptive information systems.

Hongwen Yu received his B.Eng., M.Eng. and Ph.D. degree in communication and information engineering from Shanghai University, Shanghai, China, in 2011, 2014 and 2020, respectively, and his Ph.D. degree in electronic engineering from the University of Technology Sydney, NSW, Australia in 2022. Currently, he is an Associate Professor in the Department of Communication and Information Engineering, Shanghai University. His research interests include reconfigurable intelligent surface, mmWave communications and B5G/6G wireless communications.

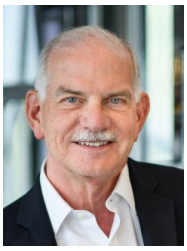

H. Vincent Poor (S'72, M'77, SM'82, F'87) received the Ph.D. degree in EECS from Princeton University in 1977. From 1977 until 1990, he was on the faculty of the University of Illinois at Urbana-Champaign. Since 1990 he has been on the faculty at Princeton, where he is currently the Michael Henry Strater University Professor. During 2006 to 2016, he served as the dean of Princeton's School of Engineering and Applied Science. He has also held visiting appointments at several other universities, including most recently at Berkeley and Cambridge. His research interests are in the areas of information theory, machine learning and network science, and their applications in wireless networks, energy systems and related fields. Among his publications in these areas is the recent book Machine Learning and Wireless Communications. (Cambridge University Press, 2022). Dr. Poor is a member of the National Academy of Engineering and the National Academy of Sciences and is a foreign member of the Chinese Academy of Sciences, the Royal Society, and other national and international academies. He received the IEEE Alexander Graham Bell Medal in 2017.

Lajos Hanzo (http://www-mobile.ecs.soton.ac.uk, https://en.wikipedia.org/wiki/Lajos_Hanzo) (FIEEE'04, Fellow of the Royal Academy of Engineering (FREng), of the IET and of EURASIP) received Honorary Doctorates from the Technical University of Budapest (2009) and Edinburgh University (2015). He is a Foreign Member of the Hungarian Science-Academy, Fellow of the Royal Academy of Engineering (FREng), of the IET, of EURASIP and holds the IEEE Eric Sumner Technical Field Award.